Palaeogeography, Palaeoclimatology, Palaeoecology 589 (2022) 110841

Contents lists available at ScienceDirect

Palaeogeography, Palaeoclimatology, Palaeoecology

journal homepage: www.elsevier.com/locate/palaeo

Impact of the Mediterranean-Atlantic connectivity and the late Miocene carbon shift on deep-sea communities in the Western Alboran Basin

Francesca Bulian [a,*], Tanja J. Kouwenhoven [b], Francisco J. Jiménez-Espejo [c,d], Wout Krijgsman [e], Nils Andersen [f], Francisco J. Sierro [a]

[a] Dept. de Geología, Univ. de Salamanca, Plaza de los Caídos s/n, 37008 Salamanca, Spain
[b] Department of Earth Sciences, Utrecht University, Princetonlaan 8a, 3584, CB, Utrecht, the Netherlands
[c] Instituto Andaluz de Ciencias de la Tierra (CSIC-UGR), Armilla, Spain
[d] Research Institute for Marine Resources Utilization (Biogeochemistry Program), JAMSTEC, Yokosuka, Japan
[e] Paleomagnetic Laboratory Fort Hoofddijk, Utrecht University, Budapestlaan 17, 3584, CD, Utrecht, the Netherlands
[f] Leibniz-Laboratory for Radiometric Dating and Isotope Research, Christian-Albrechts-Universität Kiel, Max-Eyth-Str.11-13, 24118 Kiel, Germany

ARTICLE INFO

Editor: Dr A Dickson

Keywords:
Messinian
Mediterranean circulation
Foraminifers
Stable isotopes
XRF analyses

ABSTRACT

Integration of foraminiferal and geochemical data (stable isotope and elemental composition) from West Alboran Basin (WAB) ODP Site 976 allowed evaluation of the effects of the initial Mediterranean – Atlantic restriction event preceding the Messinian Salinity Crisis (MSC) in a context of late Miocene cooling and diminishing water – mass exchange close to Gibraltar Strait.

At 7.17 Ma a prominent shift in benthic foraminifer abundances from dominantly oxic taxa to species tolerating oxygen deficiency, paired with a drop in $\delta^{13}C$ values, suggest that the restriction of the Mediterranean-Atlantic gateways profoundly affected the WAB deep waters. From 7.17 Ma onward, deep-water stagnation increased the bottom water residence time and led to oxygen depletion. Similar changes, already identified in other Mediterranean basins imply that the first signs of Mediterranean-Atlantic restriction significantly predated the onset of the MSC also in the WAB, an area sometimes considered more under the influence of the Atlantic. Simultaneously, a marked amplitude increase of several element-log ratios reveals a clear cyclical pattern related with precession. Together with new $\delta^{18}O$ data, the identification of cyclical patterns allowed improving the age model of Site 976 and consequently enabled an accurate correlation with other Mediterranean, mostly land-based sections. Comparing the records, we were able to correlate the event at a basinal scale and to refine thermohaline circulation models of the Mediterranean after 7.17 Ma.

Because this Mediterranean-scale change was contemporaneous with the global Late Miocene Carbon Isotope Shift (LMCIS) it was important to discern between global and local effects. Given the synchronicity of the global and local Mediterranean change in the $\delta^{13}C$ record, a global effect certainly affected the Mediterranean Basin. However, opposite phase relations of the global and local $\delta^{13}C$ signals with orbital parameters, paired with a higher magnitude change identified in our WAB isotope record suggests that the local imprint overruled the global one.

1. Introduction

The late Miocene was characterized by major changes in global ecosystems and climate. Between ~7.8–6.7 Ma a cooling of around 6 °C was reported (Tzanova et al., 2015; Herbert et al., 2016; Holbourn et al., 2018) contemporaneous with the Late Miocene Carbon Isotope Shift (LMCIS) characterized by a global shift in the $\delta^{13}C$ of oceanic dissolved inorganic carbon ($\delta^{13}C_{DIC}$) (Hodell et al., 1994; Hodell et al., 2001; Hodell and Venz-Curtis, 2006). On land, large-scale aridification and expansion of C_4 grasslands (Blondel et al., 2010; Edwards et al., 2010; Pound et al., 2012) led, amongst others, to the establishment of the Sahara desert (Hodell et al., 1994; Schuster, 2006; Sepulchre et al., 2006; Zhang et al., 2014; Herbert et al., 2016). During this period, the Mediterranean area was affected by an important paleogeographic

* Corresponding author.
E-mail addresses: fra.bulian@usal.es (F. Bulian), T.J.Kouwenhoven@uu.nl (T.J. Kouwenhoven), fjjspejo@ugr.es (F.J. Jiménez-Espejo), W.Krijgsman@uu.nl (W. Krijgsman), nandersen@leibniz.uni-kiel.de (N. Andersen), sierro@usal.es (F.J. Sierro).

https://doi.org/10.1016/j.palaeo.2022.110841
Received 23 August 2021; Received in revised form 17 December 2021; Accepted 6 January 2022
Available online 21 January 2022

reorganization. The Mediterranean Sea was connected to the Atlantic Ocean through the Rifian Corridor in Northern Morocco and the Betic Corridor in Southern Spain (e.g. Martín et al., 2014; Flecker et al., 2015; Achalhi et al., 2016), hosting a marine exchange significantly larger than in the present Strait of Gibraltar. However, during the Tortonian, a dynamic tectonic movement uplifted the Gibraltar Arc (Garcia-Castellanos and Villaseñor, 2011; Van den Berg et al., 2018; Capella et al., 2020) and consequently, the Betic and Rifian corridors started losing their efficiency (Krijgsman et al., 1999; Martín et al., 2014; Flecker et al., 2015; Capella et al., 2018) and progressively closed. The age of closure of the last connection through the Betic gateway (Guadalhorce Corridor) is still debated, with ages varying between late Tortonian (~7.6 Ma; Guerra-Merchán et al., 2010; Corbí et al., 2012; Van der Schee et al., 2018) and middle Messinian (6.18 Ma; Martín et al., 2001). For the Rifian corridor there is more agreement on the timing and most probably the southern strand closed between 7.1 and 6.9 Ma while the northern sectors around 7.35–7.25 Ma (Tulbure et al., 2017; Capella et al., 2018). The effects of the gateway restriction become visible in Mediterranean sediments immediately after the Tortonian – Messinian boundary, around 7.17 Ma (Seidenkrantz et al., 2000 and references therein; Blanc-Valleron et al., 2002; Kouwenhoven et al., 2003). From this time onward Mediterranean land-based sections register a shift towards benthic foraminiferal faunas indicating reduced oxygen levels (e.g., dominated by bolivinids, buliminids and uvigerinids). A parallel drop in benthic and planktic $\delta^{13}C$ (Kouwenhoven et al., 1999; Seidenkrantz et al., 2000; Kouwenhoven et al., 2003; Kontakiotis et al., 2019) testifies a profound change in Mediterranean circulation. Concurrently, the sensitivity of the basin to climatically induced changes increased, and precession-controlled fluctuations in the freshwater budget became visible in geochemical and micropaleontological records (Sierro et al., 2003), resulting in more regular sapropel deposition in the Eastern Mediterranean (Santarelli et al., 1998; Seidenkrantz et al., 2000; Hüsing et al., 2009).

Throughout the Messinian, the connections between the Mediterranean and Atlantic eventually became heavily restricted (Simon and Meijer, 2015), culminating at ~5.97 Ma (Manzi et al., 2013), with the Messinian Salinity Crisis (MSC) and widespread evaporite deposition (Hsü et al., 1973; Manzi et al., 2008; Roveri et al., 2014a). Because the closure of the Betic and Rifian gateways predates the MSC, an additional connection was necessary to regulate water inflow from the Atlantic to provide the necessary ions and trigger the MSC. Concordantly, recent studies (Capella et al., 2018; Krijgsman et al., 2018; Capella et al., 2020) suggest that a proto – Gibraltar Strait could have acted as the Mediterranean-Atlantic sill before and/or during the MSC.

In this study, we analyse the late Tortonian (7.5 Ma) – early Messinian (7 Ma) benthic foraminifer assemblages and geochemical data (both stable isotope and XRF data) from a 26 m long interval of Ocean Drilling Project (ODP) Site 976 located in the West Alboran Basin (WAB). Because the circulation of this area is strongly related with water exchange at Gibraltar Strait we aim to get a more detailed comprehension of the effects of gateway restriction at locations close to the Atlantic connections. Benthic foraminifers are great indicators of environmental conditions and, paired with $\delta^{18}O$ and $\delta^{13}C$ stable isotope records and geochemical element data, allow the reconstruction of paleoenvironments and deep – water hydrographic changes affecting the WAB before and after the 7.17 Ma restriction event initially identified at this site by Bulian et al. (2021) at 592 mbsf. The benthic $\delta^{18}O$ record allows elaborating a more accurate chronology for the late Tortonian – early Messinian at Site 976 and the benthic $\delta^{13}C$ isotopic record reveals how global and local changes affected the Mediterranean Basin. Finally, comparison between the WAB and Western and Eastern Mediterranean records allowed a Mediterranean scale perspective of the circulation changes after 7.17 Ma.

2. Study area: oceanographic setting and circulation of the modern Mediterranean

The Alboran Basin is a transitional area between the semi-enclosed Mediterranean Sea and the Atlantic Ocean that can be divided into a western (WAB) and an eastern (EAB) basin. Its circulation is very intense and strongly related with water exchange at Gibraltar Strait where the inflow of low-salinity Atlantic waters (surface water) and outflow of high salinity Mediterranean waters occur (Fig. 1). Such configuration results in two anti-cyclonic gyres: the Western and Eastern Alboran Gyres (Masqué et al., 2003 and references therein). The low saline Atlantic surface waters (salinity of 36.1–36.2‰; Rohling et al., 2015 and references therein) entering the Mediterranean flow northward towards the Gulf of Lions and eastward across the Sicily Strait reaching the Eastern Mediterranean Basin (EMB). Along this trajectory, the water becomes salty and eventually sinks in the northern Levantine basin resulting in the formation of the Levantine intermediate water (LIW; Zavatarielli and Mellor, 1995; Buongiorno Nardelli and Salusti, 2000; Pinardi and Masetti, 2000; Pinardi et al., 2019). The LIW settles between 200 and 600 m (Pinardi and Masetti, 2000) and spreads out in the entire Mediterranean. In the northern basins like the Gulf of Lions and the Adriatic and Aegean Seas (Stommel et al., 1973; Schlitzer et al., 1991; e.g. Lascaratos et al., 1999; Powley et al., 2017), surface waters are exposed to cold northerly air masses producing a strong surface buoyancy loss through cooling and evaporation, allowing the water to sink (e.g. Theocharis and Georgopoulos, 1993). Here, the interaction between the LIW and cold surface waters promotes deep water formation (Pinardi and Masetti, 2000) which is responsible for ventilation at the sea floor. These saltier (salinity of ~38.5‰; Rohling et al., 2015) intermediate waters are the main component of the Mediterranean Outflow Water (MOW) to the Atlantic Ocean (Pinardi and Masetti, 2000) and are the cause of the salinity gradient between the Mediterranean and Atlantic. This gradient triggers an anti-estuarine circulation active at least since the closure of the connection with the Indian Ocean (Karami et al., 2011).

Bottom water oxygenation in the Alboran Basin depends on the rate of deep water renewal, which is driven, in turn, by deep-water formation in the Gulf of Lions and the rate of Bernoulli aspiration exporting deep water to the Atlantic through the MOW (Stommel et al., 1973). Deep water formation depends on the Mediterranean hydrologic budget and heat exchange with the atmosphere, since the intensity of the African monsoon and Mediterranean rainfall has a strong impact on the net freshwater loss (e.g. Rohling et al., 2009; Marzocchi et al., 2015). During the last 13.5 Ma (Rohling et al., 2015 and references therein; Simon et al., 2017), the enhanced freshwater runoff (Rohling and De Rijk, 1999; Larrasoaña et al., 2003; Bianchi et al., 2006; Osborne et al., 2010; Hennekam et al., 2014) associated with stronger African monsoons during times of northern hemisphere summer insolation maxima led to greater surface productivity, water-mass stratification (Rossignol-Strick, 1985; Bosmans et al., 2015) and episodes of deep-water oxygen starvation, leading to deposition of anoxic layers (sapropels) in the EMB and organic rich layers (ORL) in the Western Mediterranean Basin (WMB; e.g. Rogerson et al., 2008; Emeis and Weissert, 2009; Rohling et al., 2015). This geographic variation is related to the different efficiency of deep – water renewal (Rohling et al., 2015). Bernoulli aspiration over a sill is dependent on the outflow velocity and density gradient below the depth of the sill (Stommel et al., 1973; Rogerson et al., 2008; Rogerson et al., 2012). Currently, because the outflow velocity at the Sicily sill is low and density stratification below the sill is high, deep water renewal of the EMB is less efficient (Rohling et al., 2015) than in the west. In the WMB, higher velocities and reduced stratification in combination with the vertical advection with the LIW, permits the flushing of deep – water masses over the Gibraltar Strait preventing sapropel formation.

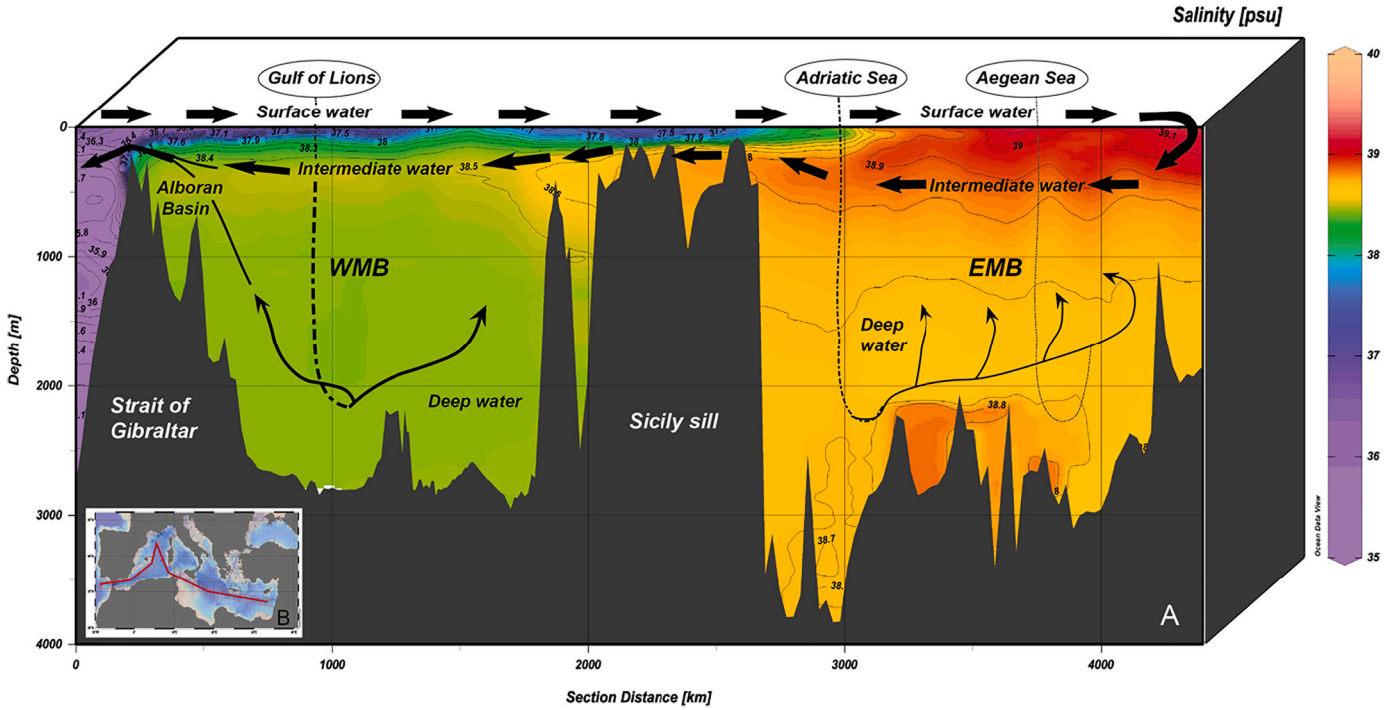

Fig. 1. (A) West to East Mediterranean Sea salinity profile produced using Ocean Data View (Schlitzer, 2015) and the general circulation of the Mediterranean Sea (arrows). Alongside to the colour coding, isohalines have been contoured to better show salinity changes. (B) The map displays the 4500 km long transect (red line) of which data (MEDARGroup, 2002) is assimilated into the profile. (For interpretation of the references to colour in this figure legend, the reader is referred to the web version of this article.)

3. Material and methods

3.1. ODP Site 976 (single Hole B)

New benthic foraminifer and geochemical data are derived from ODP Site 976 (Leg 161; 36° 12′ 18.78″ N, 4° 18′ 45.78″ W; 1108.0 m water depth), in the northern sector of the WAB (Fig. 2), ~100 km to the east of the Gibraltar Strait. The studied sediments (609–583 mbsf) are mainly composed of homogeneous nannofossil-rich claystone and nannofossil (sandy) claystone (Comas et al., 1996). The sediment does not

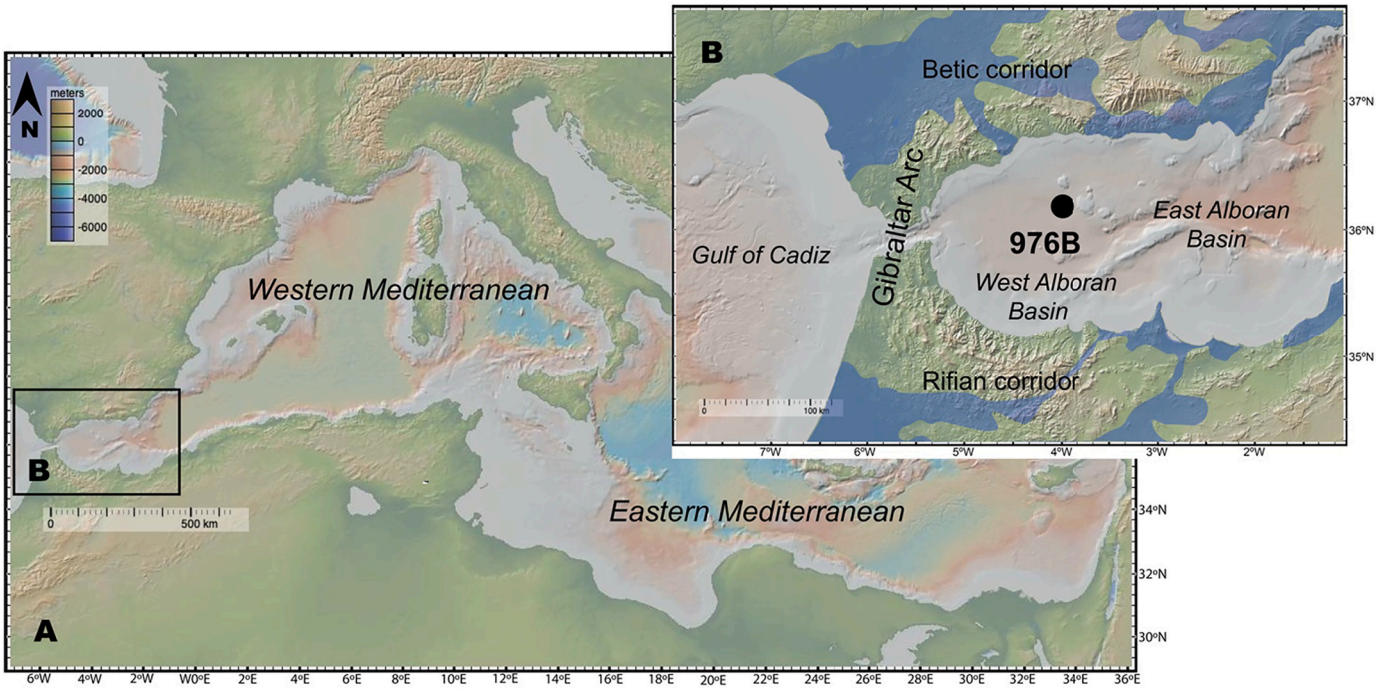

Fig. 2. (A) Topographic map of the Mediterranean Sea area and (B) topographic map of the Alboran Basin showing the location of ODP Site 976 used in this study (*http://www.geomapapp.org/*) and in blue the location of the former Betic and Rifian corridors during the late Tortonian modified after Capella et al. (2020). (For interpretation of the references to colour in this figure legend, the reader is referred to the web version of this article.)

show colour changes, but a precessionally dominated cyclicity, especially from 592 mbsf upwards (7.17 Ma), has been highlighted from X-ray fluorescence measurements and planktic foraminifer associations (Bulian et al., 2021). The analysed core sections cover the time interval from the late Tortonian (7.5 Ma) to the early Messinian (7 Ma), followed by a non-recovery interval that extends until the base of the Zanclean (~5.33 Ma). The stage boundaries are defined using planktonic foraminifer bioevents from Bulian et al. (2021).

3.2. Sample preparation

With an average sampling step of 0.3 m (~4 kyr) 93 samples were prepared for micropaleontological and geochemical analyses. The samples were dry weighed, disintegrated in water and washed over a set of 150 μm and 63 μm sieves. Studies have shown that when dealing with paleoenvironmental reconstructions there is not a significant difference between the results obtained upon analyzing the >125 μm and > 150 μm sample fractions (Weinkauf and Milker, 2018), hence, in this study the >150 μm washed residues used for planktic foraminifer analyses (Bulian et al., 2021) were selected for benthic foraminifer counts. From the same fraction, both planktic and benthic foraminifers were picked for stable isotope analyses.

3.3. Benthic foraminifer analyses

Benthic foraminifers were analysed in 59 out of the 93 samples prepared. The sampling resolution varied between 0.3 and 0.6 m resulting in an age resolution of approximately 5 to 10 kyr. Aliquots, preferably containing 150–300 benthic foraminifer specimens, were obtained using a micro splitter. The specimens were hand-picked under a dissection microscope, identified and counted. Entire samples were used when the number of foraminifers was small and samples containing less than 50 specimens were not included in the dataset. The counts were transferred to relative frequencies.

Diversity of the benthic foraminiferal assemblages has been estimated with the Shannon index, which corrects for different sample sizes, and is expressed by the formula $H = -K\sum_{i=1}^{n} pilog(pi)$ (Murray, 1991; Spellerberg and Fedor, 2003), where *pi* is the proportion of the i^{th} species and K a positive constant that takes into account the unit of measure (Shannon, 1948).

The percentage of planktic foraminifers in the foraminiferal fauna (%P) is expressed as P/(P + B)*100. The %*P* values obtained this way can be used as a first indicator of paleodepth or increasing distance to shore, where greater values indicate higher depths and vice versa (Gibson, 1989; Van der Zwaan et al., 1990). The %P is sensitive to disturbance of the deep-water environment such as hypoxia, organic flux and preferential dissolution of planktic foraminifers (Sen Gupta and Machain-Castillo, 1993b; Jorissen et al., 1995; Loubère, 1996; Kucera, 2007; Nguyen et al., 2011), factors affecting the reliability of %P. To avoid the effect of hypoxia, Van der Zwaan et al. (1999) and Van Hinsbergen et al. (2005) suggest excluding infaunal foraminifer species (i.e. species living in the sediment). In this study, the %P values have been estimated with and without infaunal species (i.e. *Globobulimina* spp., *Chilostomella* spp. and all species of the genus *Uvigerina*, *Bulimina* and *Bolivina*) and both paleodepth estimates have been compared with literature data on depth limits of benthic foraminifers (e.g. Pérez-Asensio et al., 2012a, 2012b and references therein).

Benthic foraminiferal accumulation rates (BFARs) were used as a paleoproductivity proxy because fluctuations were found to indicate changes in surface productivity and nutrient fluxes (Herguera, 1992; Herguera, 2000). BFARs were calculated from the product of the number of benthic foraminifers per gram of dry sediment (BF/g), the sedimentation rate (cm/kyr) estimated in Bulian et al. (2021) and dry bulk density (g/cm^3) interpolated from shipboard physical properties data in ODP Initial Reports for Site 976 (Comas et al., 1996).

Because infaunal foraminifers become more abundant under low-oxygen conditions and/or high organic matter fluxes while epifaunal species (i.e. living at or on top the sediment-water interface) are less tolerant to low-oxygen levels (e.g. Corliss and Chen, 1988; Jorissen et al., 1995; Gooday, 2003), the epifaunal/infaunal ratio (E/I) can highlight changes in bottom-water oxygenation. This ratio is expressed as E/(E + I) where E is the sum of the relative abundances of epifaunal and I of infaunal benthic foraminifers.

Since the sediments were deposited at bathyal depth (Section 5.2), the sum of displaced shallow-water benthic foraminifer species including *Elphidium* spp., *Rosalina* spp., discorbids and *Cibicides lobatulus* (Supplement 1) was used as an indicator of downslope transport. Usually, a higher number of displaced individuals is linked with intense currents (Fentimen et al., 2020 and references therein) that can efficiently transport these shallow water, sometimes epiphytic species (Langer, 1993) to deeper parts of the basin.

In order to gain insight in the variations of the benthic species assemblages through time, a Principal Components Analyses (PCA) was performed using Past 4.02 software (Hammer et al., 2001). The most abundant (≥ 3%) 24 variables were introduced into the analysis, consisting of species, genera and higher order categories. Single and fragmentary occurrences and ill-defined rest groups were removed from the data. To identify species groups presenting similar trends and hence occurring in similar environments, a hierarchical cluster analyses (Pearson correlation: Past 4.02 software; Hammer et al., 2001) was performed including the same 24 variables. When species from a genus were scarcely present, but a genus as a whole considered indicative of analogous environmental conditions, their sum was utilized. *Cancris* spp. contains the species *C. oblongus* and *C. auriculus*, *Bolivina dilatata* is the sum of *B. dilatata* and *B. spathulata*, while in *Pullenia quinqueloba* group, both forms with four and five chambers were included. Because unilocular and uniserial hyaline foraminifers were very diverse but each taxon occurred in low abundances, they were taken together in the unilocular + uniserial group which comprises unilocular taxa, including *Lagena* and *Procerolagena* spp., *Nodosaria* spp., and *Pseudonodosaria* spp.

3.4. Geochemical analyses

3.4.1. Stable isotopes

From the washed residues of all 93 samples prepared, between 10 and 20 specimens of the planktic foraminifer *Globigerina bulloides* were picked and cleaned ultrasonically for oxygen and carbon stable isotope analyses. Even after the cleaning, some specimens were still cemented by calcite and therefore 34 samples were discarded (21 from the intervals 599.80–600.39 mbsf; 596.06–598.07 mbsf; 592.84–594.33 mbsf and 13 irregularly distributed from 601 mbsf downward). Of the benthic foraminiferal content, 2 to 10 specimens of *Cibicidoides kullenbergi* were picked and analysed for oxygen and carbon isotopes. The analyses were performed with a Finnigan MAT 253 mass spectrometer connected to a Kiel IV carbonate preparation device at the Christian-Albrechts University in Kiel (Germany). Sample reaction was induced by individual acid addition (99% H_3PO_4 at 75 °C) under vacuum. The evolved carbon dioxide was analysed eight times for each individual sample. As documented by the performance of international [NBS19: +1.95‰ VPDB (^{13}C), −2.20‰ VPDB (^{18}O); IAEA-603: +2.46‰ VPDB (^{13}C), −2.37‰ VPDB (^{18}O)] and laboratory-internal carbonate standards [Hela1: +0.91‰ VPDB (^{13}C), +2.48‰ VPDB (^{18}O); HB1: -12.10‰ VPDB (^{13}C), −18.10‰ VPDB (^{18}O); SHK: +1.74‰ VPDB (^{13}C), −4.85‰ VPDB (^{18}O)], analytical precision of stable isotope analysis is better than ±0.08‰ for $\delta^{18}O$ and better than ±0.05‰ for $\delta^{13}C$. The obtained values were calibrated relative to Vienna Pee Dee Belemnite (VPDB).

The gradient between the benthic and planktic $\delta^{13}C$ ($\Delta\delta\ ^{13}C$) was calculated. Doing so, it is important to consider that a foraminifer shell reflects the $\delta^{13}C$ composition of the dissolved inorganic carbon of the seawater where it calcifies, but usually not in isotopic equilibrium with seawater (Hillaire-Marcel and Ravelo, 2007). Therefore, it is necessary

to correct the $\delta^{13}C$ values for the deviation from equilibrium caused by the vital effect before discussing absolute values. In the case of *G. bulloides*, we compared ODP Site 976 data with values measured for the present-day water column and core tops (modern sediment samples) of the Alboran Sea region. Core top $\delta^{13}C$ data of *G. bulloides* from ODP Site 977 in EAB yield an average value of −0.75‰ (Pérez-Folgado et al., 2004), and core top studies from WAB core HER-GC-UB-6 show values of about −0.5‰ (Pérez-Asensio et al., 2020), whereas present-day surface waters from the Alboran Basin show values of around 1.4‰. The total negative disequilibrium of the $\delta^{13}C$ reported in *G. bulloides* tests amounts to ~2‰ (in agreement with laboratory studies; Spero and Lea, 1996), the difference between −0.6‰ as the $\delta^{13}C$ core-top average and 1.4‰ from the surface waters. The planktic isotope values were therefore adjusted by adding 2‰ ($\delta^{13}C$ planktic corrected). The $\delta^{13}C$ measurements obtained on *Cibicides kullenbergi* do not need any corrections, because this species precipitates in isotopic equilibrium with bottom water (Wefer and Berger, 1991; Hodell et al., 2001; Hillaire-Marcel and Ravelo, 2007).

3.4.2. Major elements

For the elemental analyses, the archive half of the core was scanned with an XRF Avaatech core scanner at MARUM (Research Faculty,

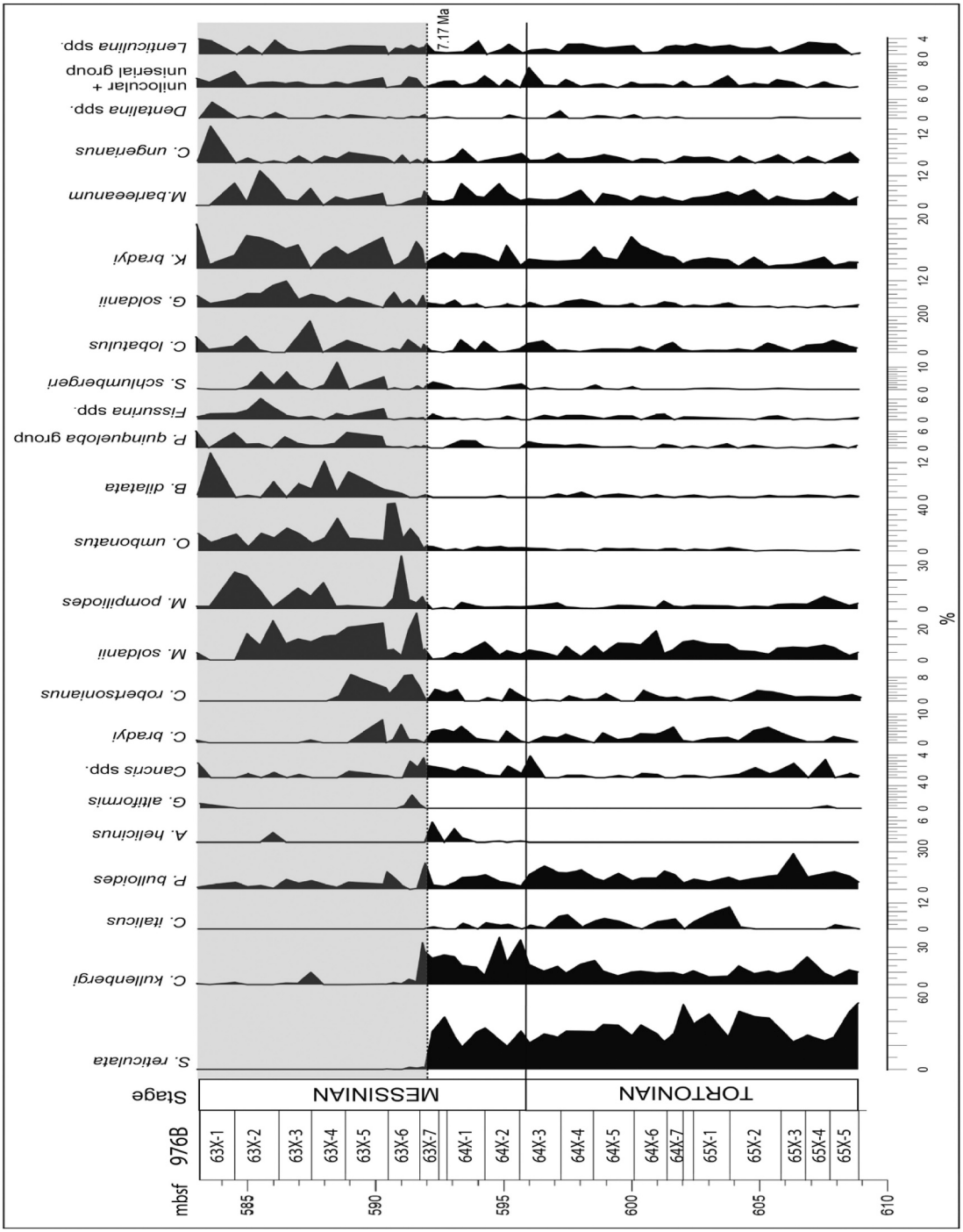

Fig. 3. Relative abundances of the benthic foraminifer species ≥3% selected for the statistical analyses against depth and stages of Site 976. The continuous black line highlights the Tortonian – Messinian boundary while the dashed line and the grey band highlight the 7.17 Ma restriction event.

Bremen University, Germany). The data reported here have been acquired by a Canberra X-PIPS Silicon Drift Detector with 150 eV X-ray resolution, the Canberra Digital Spectrum Analyzer DAS 1000, and an Oxford Instruments 50 W XTF5011 X-Ray tube with rhodium (Rh) target material. Due to the bad core preservation and occasional intercalations of perforating mud, the sampling steps were inserted manually ranging between 1 and 7 cm (0.2–1 kyr). To detect both light and heavy elements, two runs were performed, the first using generator settings of 30 kV, current of 1.0 mA and a sampling time of 15 s, while the second run was performed with 10 kV, 0.2 mA and 10 s sampling time. Because the obtained data are not quantitative, but are expressed in counts, element-log ratios are preferred for the data interpretation (Weltje and Tjallingii, 2008; Rothwell, 2015). Considering the conservative behaviour and terrigenous origin of aluminum (Calvert and Pedersen, 2007; Martinez-Ruiz et al., 2015), Al – normalization was used following other geochemical studies of high detrital input areas like the WMB and EMB (e.g. Jimenez-Espejo et al., 2007; Rodrigo-Gámiz et al., 2014; Martinez-Ruiz et al., 2015). In this study the following element – log Al – normalized ratios have been used: titanium/aluminum (Ti/Al), potassium/aluminum (K/Al), rubidium/aluminum (Rb/Al) alongside with the titanium/calcium (Ti/Ca) and sulphur/titanium (S/Ti) element – log ratios (Bahr et al., 2005; Hoang et al., 2010; Harff et al., 2011). The Principal Component Analyses performed on this dataset was published in Bulian et al. (2021),while the element – log normalized ratios are shown in this study.

3.5. Spectral analyses

Spectral analysis was performed on the benthic $\delta^{18}O$ and $\delta^{13}C$ record and element log ratios in order to identify the nature and significance of the periodic changes present. The spectral analysis was carried out in depth and time domain using PAST software (Hammer et al., 2001) on evenly resampled datasets. Frequency peaks over 95% confidence were considered significant.

4. Results

4.1. Distribution of benthic foraminifer assemblages

The data set contains 76 taxa (Supp. 1). The distribution of the benthic foraminifer species with abundances ≥3% is shown in Fig. 3.

4.1.1. 608.9 to 592 mbsf

The lowermost 17 m of the studied interval covers the upper Tortonian and lower Messinian (Fig. 3) and includes the Tortonian/Messinian boundary at 596 mbsf (first common occurrence (FCO) of the planktic species *Globorotalia miotumida* group; Bulian et al., 2021).The benthic foraminifer assemblages are well preserved and moderately diversified. The record is dominated by *Siphonina reticulata* (up to 60%), with *Pullenia bulloides* and *Cibicidoides kullenbergi* both reaching 30% of the total abundance (Fig. 3). Accessory species (5–10%) are *Cibicidoides italicus*, *Cibicides robertsonianus*, *C. lobatulus, C. ungerianus, Melonis pompilioides, Melonis barleeanus* and *Karreriella bradyi*. *Anomalinoides helicinus* is found only in the topmost 2 m of this interval.

4.1.2. 592 to 583.12 mbsf

Above 592 mbsf several benthic species disappear (e.g. *C. italicus*, *S. reticulata* and *C. kullenbergi*), while others increase (e.g. *M. soldanii*, *M. pompilioides*, *Oridorsalis umbonatus*, *B. dilatata*; Fig. 3). A sharp peak in the abundance of *M. soldanii* (30%) is followed with a slight delay by *M. pompilioides* (up to 30%) and high frequencies (≥ 40%) of *O. umbonatus*. Other taxa showing a clear increase in abundance are *Sigmoilopsis schlumbergeri*, *Fissurina* spp., *P. quinqueloba, B. dilatata* and *K. bradyi*, the latter reaching 20% abundance. A gradual increasing upward trend can be identified in *Gyroidina soldanii* and *M. barleeanus*. *Cibicidoides bradyi* and *C. robertsonianus* show an initial increase in frequency, not exceeding 6%, before disappearing completely above 588 mbsf.

4.2. Paleoecological and statistical parameters of the benthic foraminifer assemblage

The paleoecological and statistical parameters used in this study are shown in Fig. 4 and can be found in Supp. 2. The %P curves both with and without the infaunal benthic species, show an analogous behaviour (Fig. 4 a) and remain fairly constant until 592 mbsf when two episodes with lowered %P are registered (at 591 and 587.5 mbsf), the youngest corresponding with the highest (20%) peak of displaced foraminifers. The sum of displaced benthic foraminifers (Fig. 4 b) fluctuates between 2% and 14% with a 20% peak at 587 mbsf. The Shannon diversity index (Fig. 4 c) shows a slight upward increasing trend, with large shifts in values from the base to 590 mbsf when it remains constant towards the top of the studied core section. Simultaneous with the shift in the benthic foraminifer assemblage, the E/(E/I) ratio (Fig. 4 d) displays a radical drop in values above 592 mbsf which persists until the top of the record. The BFAR values show relatively large variations around the mean of ~200 benthic foraminifera/cm^2/kyr throughout most of the Tortonian (Fig. 4 e). Towards the Tortonian-Messinian boundary values increase and at 592 mbsf, they gradually start to decrease, and stabilize around lower values (~100).

4.3. Statistical analysis of the benthic foraminifer assemblages

The Principal Components Analyses (PCA; Supp. 2) yields two statistically significant components, PC1 and PC2, together explaining 63.6% of the variance within the dataset (48.12% on PC1 and 15.15% on PC2). The third and further axes explain less than 10% of the variance and are not considered. The loadings, i.e. the contribution of each individual variable on a component (axis), are given in Table 1. The two most positive loadings for PC1 are *S. reticulata* and *Cibicides kullenbergi* while the negative ones are *M. pompilioides, M. barleeanum* and *O. umbonatus* (Table 1).

The positive loadings for PC2 are *S. reticulata* and *O. umbonatus* together with *M. soldanii*, and the most negative loadings on PC2 are of *Cibicides kullenbergi* and *P. bulloides*. From PC1 and PC2 (Fig. 4) two major faunal assemblages can be identified. The first one is associated with upper Tortonian-lowermost Messinian samples (until 592 mbsf) and is characterized by species loading positively on PC1 such as *S. reticulata* and *C. italicus,* and species loading negatively *C. kullenbergi* and *P. bulloides*. The second assemblage characterizes the Messinian deposits from 592 mbsf upwards and is dominated by *O. umbonatus* and *M. soldanii* loading positively and *M. pompilioides* loading negatively on PC2.

The dendrogram (Fig. 5; Supp. 2) highlights the clear partition between the pre- and post- 592 mbsf assemblages as well as the changes in species distribution reflected in Cluster 2. Above 592 mbsf, a first increase in Cluster 2A (*C. brady, Cibicides robertsonianus* and *A. helicinus*) is visible related with the establishment of clear cyclical juxtaposition between Clusters 2D (*Cibicides lobatulus* and *M. pompilioides*) and 2C (unilocular+uniserial group, *P. quinqueloba* group, *Cancris* spp., *M. barleeanum*, *M. soldanii*, *Sorghum schlumbergeri*, *Fissurina* spp., *Karreriella bradyi*, *G. soldanii* and *O. umbonatus*). Cluster 2B (*Lenticulina* spp., *B. dilatata*, *Dentalina* spp. and *C. ungerianus*) is present throughout the record, with a peak at the topmost part of the studied interval.

4.4. Oxygen and carbon isotope records

Throughout the Tortonian and the lowermost Messinian, both $\delta^{18}O$ curves display a general trend towards heavier values, which is more accentuated in the benthic $\delta^{18}O$ record (Fig. 6 d,e; Supp. 3). Both records show a decrease between 592 and 588 mbsf. The planktic $\delta^{13}C$ record (Fig. 6 a) displays a general stable trend fluctuating around the mean

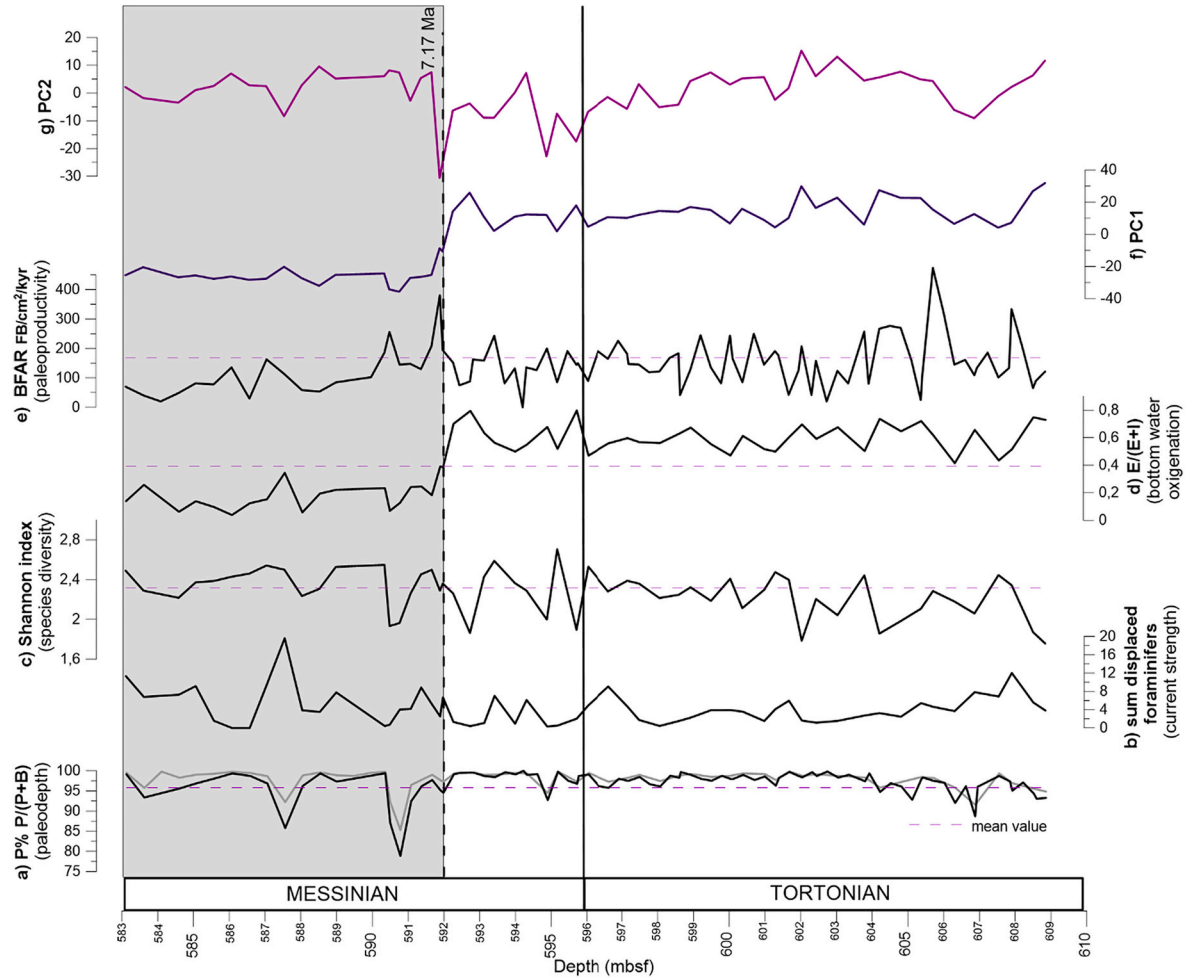

Fig. 4. The obtained paleoecological and statistical parameters for Site 976: a) The percentage of planktic foraminifers estimated with benthic infaunal species (in black) and without them (in grey; P%); b) Sum of displaced benthic foraminifers; c) Shannon index; d) Epifaunal/Infaunal ratio (E/(E + I)); e) Benthic foraminifers accumulation rate (BFAR); f) First Principal Component (PC1); g) Second Principal Component (PC2); Both Principal components reflect the change in benthic foraminifer assemblage before and after the 7.17 ma event. The grey rectangle highlights these changes. The full bleck line highlights the Tortonian – Messinian boundary while the dashed one the 7.17 Ma restriction event.

Table 1
PCA loadings for the species imported into statistical analyses of Site 976.

Species	PC1	PC2
A. helicinus	0.0027376	−0.016628
B. dilatata	−0.061295	0.024992
C. brady	0.024318	0.010516
C. italicus	0.037679	0.027948
Cibicides kullenbergi	0.25215	−0.78923
Cibicides lobatulus	−0.03673	−0.014036
Cibicides robertsonianus	−0.018294	0.045272
C. ungerianus	0.0016942	−0.0062112
Cancris spp.	−0.0002538	−0.039412
Dentalina spp.	−0.0084259	−0.0077934
Fissurina spp.	−0.018795	0.019156
G. altiformis	−0.0027291	−0.017681
G. soldanii	−0.07641	−0.0092862
Karreriella bradyi	−0.086638	0.066844
Lenticulina spp.	−0.0049852	−0.0012906
M. barleeanum	−0.0011975	−0.04937
Melonis pompiloides	−0.17122	−0.069048
M. soldanii	−0.13135	0.28641
Nodosaria spp.	−0.012546	0.020032
O. umbonatus	−0.38708	0.26736
P. bulloides	0.079487	−0.17932
P. quinqueloba	−0.030854	0.0078701
S. reticulata	0.84227	0.41526
Sorghum schlumbergeri	−0.043736	0.020137

value of ~0‰ (~2‰ when corrected) throughout the Tortonian and Messinian. The benthic $\delta^{13}C$ values vary between +1 and − 1.8‰ showing a significant negative excursion of ~1‰ starting at 592 mbsf, and a mean value around −1‰ persists until the top of the record. The sharp negative benthic $\delta^{13}C$ drop, in comparison with the stable planktic $\delta^{13}C$ is evident in the $\Delta\delta^{13}C$ gradient curve (Fig. 6 c), which increases from 1.5‰ below 592 mbsf to 2.8‰ above this depth. The benthic and planktic $\delta^{13}C$ records are in phase as well as the $\delta^{18}O$ curves and show a general cyclical behaviour throughout the entire section. The same phase relationship between all four datasets is also visible.

4.5. Semiquantitative elemental geochemistry

All the semiquantitative elemental data and the normalized element – log ratios used in this research can be found in Supp. 4. The Zr/Al ratio (Fig. 7 a) oscillates around a mean of −0.1 throughout the uppermost Tortonian and lower Messinian. At 592 mbsf the values sharply increase and so do the oscillation amplitudes. The Zr/Al, Ti/Al and Rb/Al (Fig. 7 a,b,c) curves show overall a similar trend, with a sharp increase at 592 mbsf. The Ti/Ca ratio (Fig. 7 d) decreases from the bottom up to 593 mbsf when the values and amplitudes increase and stay high throughout the rest of the record. The S/Ti ratio (Fig. 7 e) shows a generally oscillating and upward increasing trend in three steps, with increasingly higher values especially above 592 mbsf and the largest peak in the

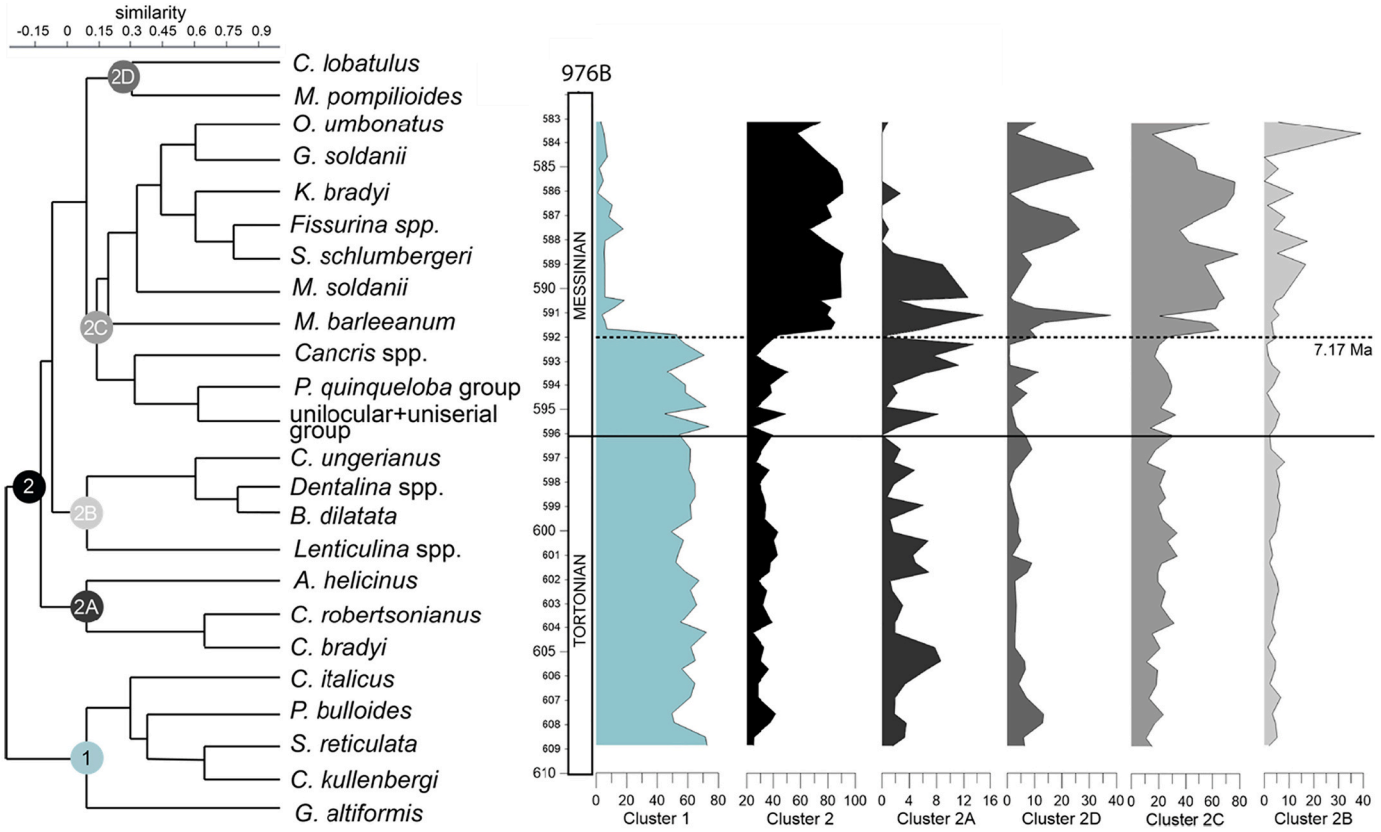

Fig. 5. Dendrograms resulting from hierarchical clustering that divided the benthic faunas into two main clusters (Cluster 1 and 2) and four sub clusters (Cluster 2A, 2B, 2C and 2D). All the cluster have been plotted against depth on the right hand side. The continuous black line highlights the Tortonian – Messinian boundary while the dashed one the 7.17 Ma restriction event.

uppermost part of the Messinian record, just below the non-recovery interval. An analogous phase relationship can be seen in the Zr/Al, Ti/Al, Rb/Al and Ti/Ca ratios.

5. Discussion

5.1. Improved age model

5.1.1. Mechanisms driving the sedimentary cyclicity before and after the 7.17 Ma restriction event

The cyclical patterns of the sedimentological and micropaleontological record, especially in the interval 592–583.12 mbsf, have been discussed in Bulian et al. (2021). The sedimentological record of the interval before 592 mbsf (7.17 Ma) did not show a clear cyclicity and therefore a precise cycle to cycle tuning was not possible using the foraminifer assemblages. However, the cyclical changes in planktic oxygen isotopes in the Mediterranean mainly reflect freshwater budget oscillations and sea surface temperatures as warmer temperatures and humid climates result in lighter oxygen isotope ratios (Lourens et al., 1996; Rohling and Cooke, 1999; Lisiecki and Raymo, 2005), while benthic carbon isotopes reflect changes in organic carbon remineralization that are, in turn, driven by variations in deep water ventilation and organic carbon flux to the seafloor (Laube-Lenfant and Pierre, 1994; Pierre, 1999). Hence, the new stable isotope records can be used to elaborate a more accurate age model of the entire record. Concordantly, the cyclical pattern in the newly acquired stable isotope data is evident both before and after 592 mbsf and it has been confirmed by spectral analyses which yielded cycles of 6.6 m and 1.4 m for the lower interval (592–609 mbsf) and of 3.3 m and 2 m for the upper interval (583–592; Fig. 8).

Below 592 mbsf the geochemical cycles visible in the $\delta^{18}O$ and $\delta^{13}C$ record covary (Fig. 9). In the 592–609 mbsf interval, maxima of planktic and benthic $\delta^{18}O$ were linked to summer insolation minima assuming they are correlated with lower rates of Nile discharge and decreasing annual rainfall, causing increasing surface salinities and lower surface temperatures (Bosmans et al., 2015; Rohling et al., 2015 and references therein). The resulting enhanced surface densities favour vertical mixing and deep – water formation enabling a good ventilation that should result in high benthic $\delta^{13}C$ values associated with insolation minima. During these times, the lower rainfall in the Alboran watersheds should also result in lower river supply of detrital elements (e.g. Ti, Rb, Zr, Si) to the basin. Here, however, an opposite behaviour is observed. Higher detrital element supply (higher Ti/Ca, Rb/Al, Ti/Al and Zr/Al ratios, e.g. Fig. 9) are associated with high planktic and benthic $\delta^{18}O$ and high benthic $\delta^{13}C$, suggesting an unexpected higher detrital input at times of insolation minima. If river supply as the source of clastic particles is ruled out, terrigenous particles must necessarily derive from wind-blown dust from north Africa (e.g. Calvert and Pedersen, 2007; Martinez-Ruiz et al., 2015). Analogous phase relations were found in the Trubi formation in Sicily (beige layers signal of Trubi formation; De Visser et al., 1989) and in EMB Site 967 (Leg 160; Larrasoaña et al., 2003 and references therein; Konijnendijk et al., 2014), where most of the detrital input occurs during insolation minima. The clastic particles were not supplied by rivers, but by wind-transported dust from North Africa, strongly diluting the carbonate content of the sediments.

By contrast, above 592 mbsf higher detrital element supply (high Ti/Ca, Zr/Al, Ti/Al or Rb/Al) covaries with lighter planktic and benthic $\delta^{18}O$ and $\delta^{13}C$ (Fig. 9). Here, higher values of these ratios are linked to insolation maxima when humid conditions dominate the Mediterranean and high annual precipitation and enhanced riverine discharge (Rohling et al., 2015 and references therein) promote water column stratification and the proliferation of warm oligotrophic water planktic foraminifer

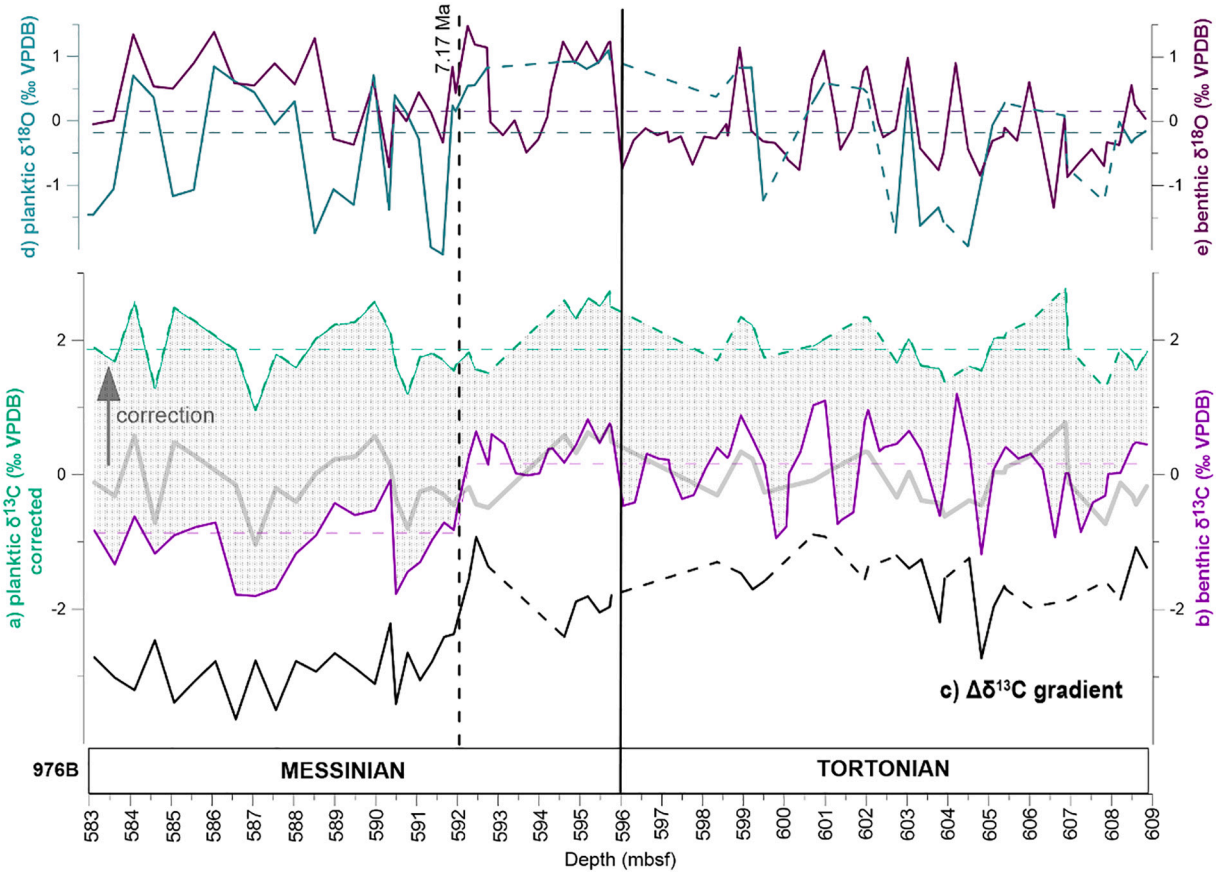

Fig. 6. Upper Tortonian and lower Messinian stable isotope curves from ODP Site 976: a) corrected planktic (*Globigerina bulloides*) $\delta^{13}C$ curve (original curve in grey); b) benthic (*Cibicides kullenbergi*) $\delta^{13}C$ curve; c) benthic – planktic $\Delta\delta^{13}C$ carbon gradient; d) planktic (*G. bulloides*) $\delta^{18}O$ isotopic record; e) benthic (*C. kullenbergi*) $\delta^{18}O$ isotopic record. The dashed lines indicate the mean value while the planktic record discontinuous lines shows intervals where planktic data could not be measured due to intense calcification. The black line shows the Tortonian – Messinian boundary while the dashed one highlights the 7.17 Ma restriction event.

species (WOWPF) together with an enrichment in detrital elements (Ti, Zr, Rb; Fig. 9). Contemporaneously, low salinity surface water prevents deep water formation and ventilation of the bottom resulting in increased bottom water residence time, evidenced by lighter benthic $\delta^{13}C$ values. Above 592 mbsf, during insolation minima cold eutrophic water planktic species (CEWPF; Fig. 9) co-occur with sediments enriched in biogenic elements (Ca and Sr; Bulian et al., 2021) and light $\delta^{18}O$ and $\delta^{13}C$ values. These cycles can be interpreted as dilution cycles where fluvial detrital input replaced eolian dust as the main diluting factor. Cyclical behaviour can also be seen in at least the first three insolation maxima in the benthic foraminifer record. The increase of Cluster 2D, dominated by allochthonous *Cibicides lobatulus*, together with *M. pompilioides* (Fig. 9), known to proliferate when levels of terrestrial refractory organic matter are high (Poli et al., 2012 and references therein), can be explained by the increased terrigenous/fluvial input coming to the basin. Similar orbitally-driven climatic alternations were described in the Sorbas (Vázquez et al., 2000; Sierro et al., 2003), Gavdos Basins (Seidenkrantz et al., 2000; Pérez-Folgado et al., 2003) and the Balearic promontory (Frigola et al., 2008), while Greek, and Italian sections (Seidenkrantz et al., 2000; Krijgsman et al., 2002; Hüsing et al., 2009; Di Stefano et al., 2010) show an alternation between normal marine and sapropel sedimentation (Section 5.4). In addition, a similar climate signature and cyclicity has been observed in Atlantic locations proximal to the Mediterranean like SW Spain and NW Morocco (Van Der Laan et al., 2012; Van den Berg et al., 2015).

5.1.2. Astronomical tuning of the geochemical record

First order calibration of the benthic and planktic $\delta^{18}O$ curves of Site 976 was achieved using foraminifer bioevents and stage boundaries from Bulian et al. (2021). Reliable bioevents include the FCO of planktic *Globorotalia menardii* 5 group at 601.96 mbsf, the FCO of *G. miotumida* group at 594.9 mbsf and the disappearance of *Globorotalia suterae* at 592 mbsf (Bulian et al., 2021) (Fig. 10). The *Globorotalia suterae* event has been astronomically calibrated at 7.17 Ma (Lirer et al., 2019). The *G. menardii* 5 group event has been calibrated at 7.36 Ma and the *G. miotumida* group event at 7.24 Ma (Lirer et al., 2019) and have been recorded respectively in cycle 11 and 16 of the Faneromeni section in Crete (grey marls, Fig. 10) (Krijgsman et al., 1994; Hilgen et al., 1995; Santarelli et al., 1998) and cycle 9 and 15 of Oued Akrech section in Morocco (reddish layers) (Hilgen et al., 2000). In the two sections, these cycles have been correlated with Northern Hemisphere summer insolation maxima phases (Krijgsman et al., 1994; Hilgen et al., 1995; Santarelli et al., 1998). In the Faneromeni section, the insolation maxima peak between cycle 17 and 18 does not materialize while in the Oued Akrech section it is represented by cycle 17 (Fig. 10). Considering that the cyclicity at 976 Site is also driven by precession (1.4 and 2 m cycles while the 3.3 and 6.6 m cycle are related to other orbital parameters), we used the cycles identified in the two sections as an aid for astronomical tuning. For the lower part of the record (592–609 mbsf), the insolation maxima peaks corresponding to the grey layers in Faneromeni section (cycles F7 to F18) and reddish intervals in Oued Akrech section (cycles OA5 to OA18) were related with $\delta^{18}O$, $\delta^{13}C$ and Ti/Ca minima. In the upper part of the core (583–592 mbsf) insolation maxima phases derived from $\delta^{18}O$, $\delta^{13}C$ and CEWPF minima and Ti/Ca, WOWPF and benthic Cluster 2D maxima and were related with cycles F18 – F23 of Faneromeni section and Cycles OA18 – OA21 in Oued Akrech secton (Fig. 10). The evident change in sedimentation rates visible after the tuning are probably the cause of the different phase relationship before and after

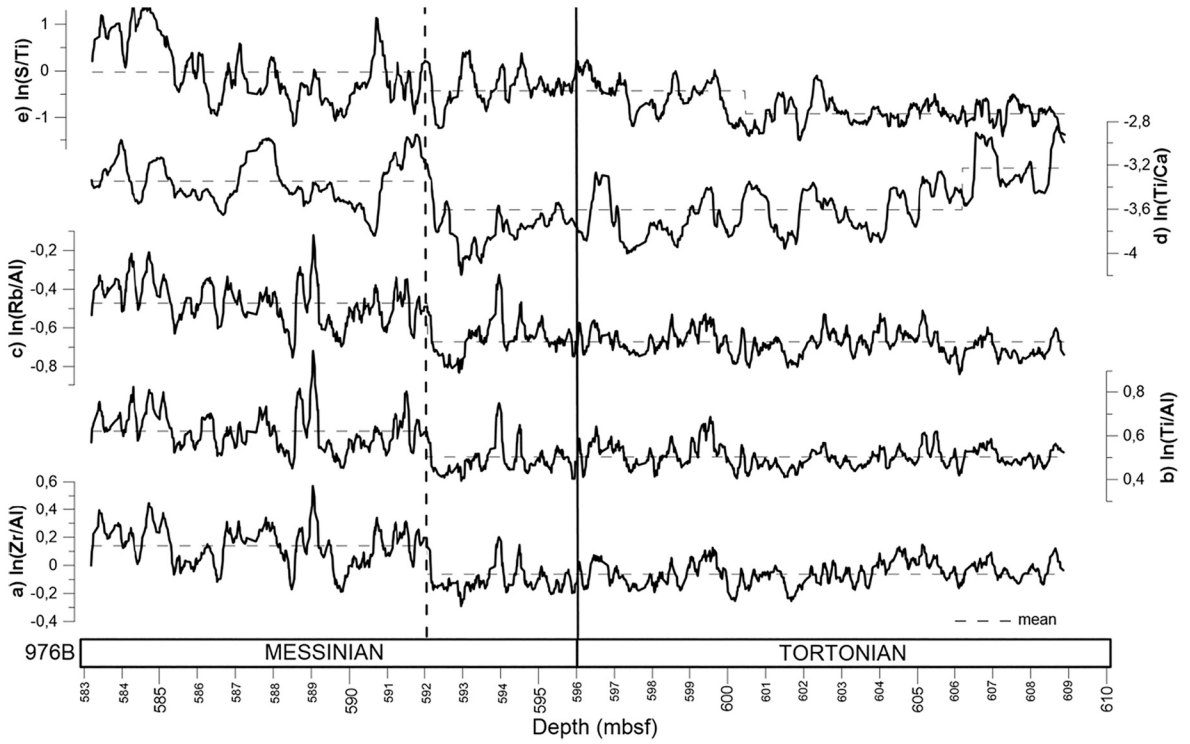

Fig. 7. Proxies derived from geochemical data of ODP Site 976: a) ln(Zr/Al) ratio; b) ln(Ti/Al) ratio; c) ln(Rb/Al) ratio; d) ln(Ti/Ca) ratio and e) ln(S/Ti) ratio. The black line shows the Tortonian – Messinian boundary while the dashed one highlights the 7.17 Ma restriction event.

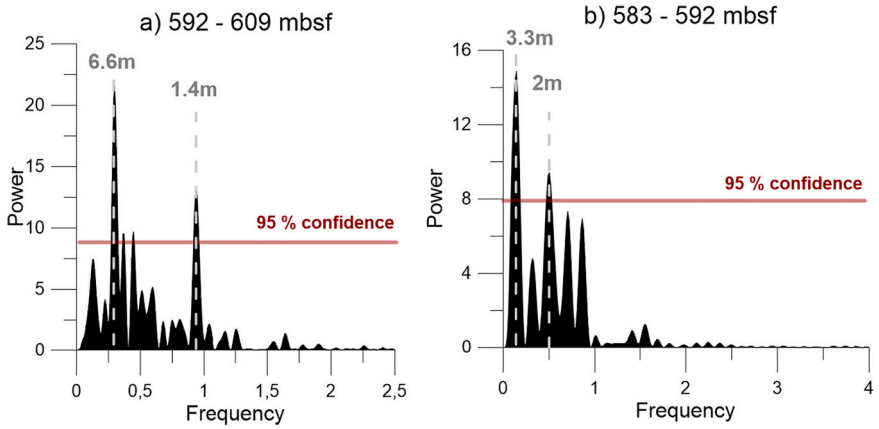

Fig. 8. Power spectrum of the benthic $\delta^{18}O$ record of Site 976 before and after the restriction event at 592 mbsf with the main cyclicities expressed in meters. Th 95% confidence interval is indicated by the red line. (For interpretation of the references to colour in this figure legend, the reader is referred to the web version of this article.)

the 7.17 Ma event (Fig. 10).

5.2. Paleo-water depth reconstruction

Based on a mean %P between 95 and 100% (Fig. 4), the calculated paleodepth using the transfer function in Van der Zwaan et al. (1990) and Van Hinsbergen et al. (2005) would be ~1000–1200 m. This is in fact the maximum paleodepth that can be resolved with this method, so extra constraint is needed. Many benthic foraminifers occupy a considerable depth range, but some species or species groups can give an indication of paleo-water depth. Amongst the most abundant benthic foraminifer species recorded in the late Tortonian-early Messinian part of the record (608.9–592 mbsf) are *S. reticulata* and *Cibicides kullenbergi*, together with *C. italicus* and *Cibicides robertsonianus,* considered epifaunal species occurring at middle bathyal water depths (Wright, 1978; Sgarrella and Moncharmont Zei, 1993; Schönfeld, 1997; Violanti et al., 2011; Pérez-Asensio et al., 2012a, 2012b). The third most common taxon, *P. bulloides*, has been reported from neritic to abyssal water depths (200–4000 m; Pelum et al., 1976; Pflum et al., 1976; Bornmalm, 1997) but is usually considered a deep-water taxon (e.g. Mackensen et al., 1985; Van Marle, 1988; Mackensen et al., 1993). Mesobathyal depths have not been uniformly defined and environmental parameters are more instrumental than water depth (e.g., Jorissen et al., 2007). In addition, the bathyal range is more condensed in the Mediterranean than in the open ocean (Bandy and Chierici, 1966). Here, water depths between ~500 and ~2000 m are considered mesobathyal (differing from for instance Wright, 1978, who considers epibathyal and mesobathyal, and Schönfeld, 1997, who considers upper- and lower bathyal depths). Considering the abundances of *C. kullenbergi and S. reticulata* and the near absence of *Cibicides wuellerstorfi*, which has an upper depth

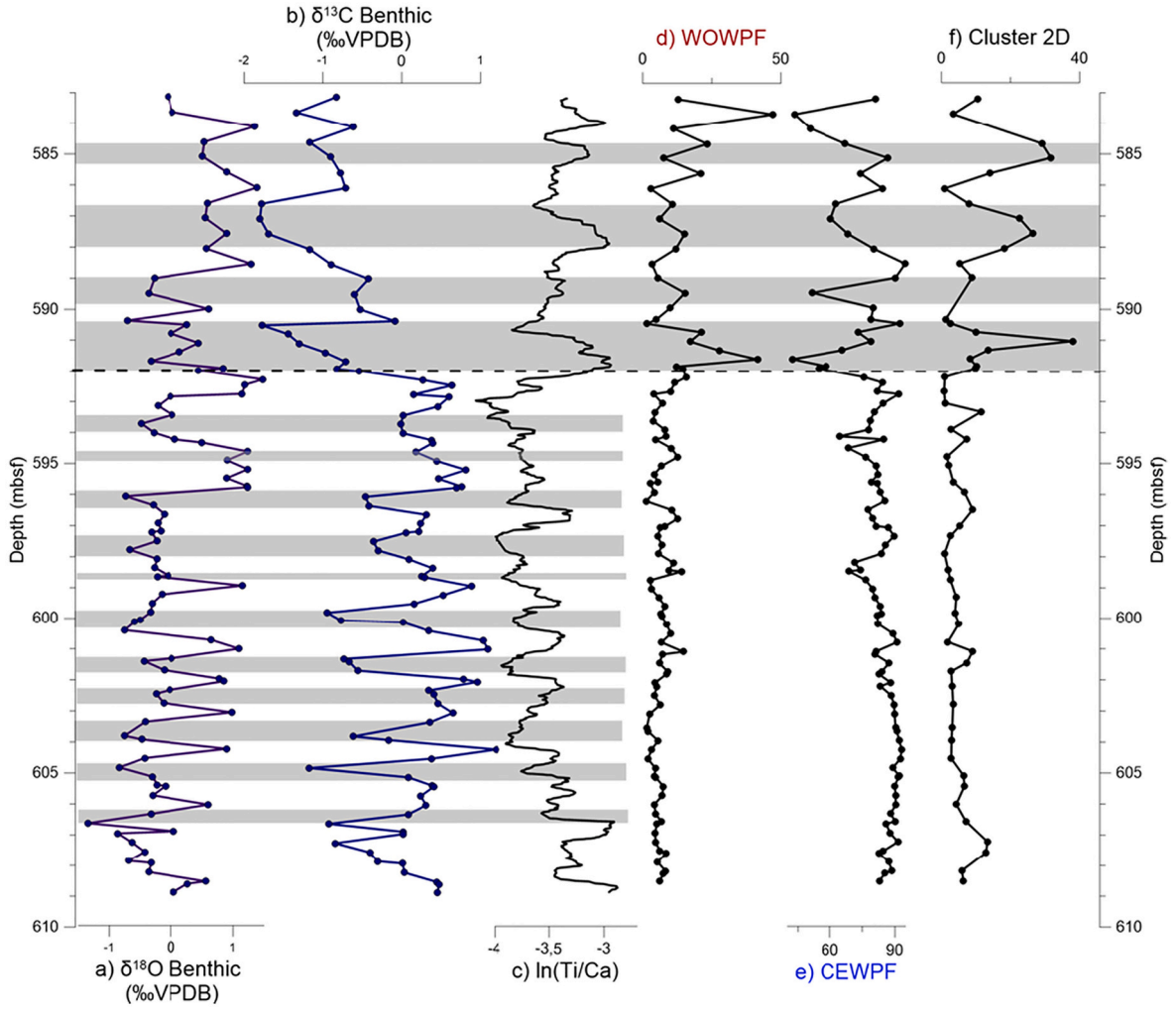

Fig. 9. Precessionally driven cyclicity evident in the ODP Site 976 record shown in depth domain. From left to right: a) benthic $\delta^{13}C$ curve; b) benthic $\delta^{18}O$ curve (benthic curves are used because the record is more continuous); c) ln(Ti/Ca) ratio; d) the sum of warm oligotrophic water planktic foraminifer species (WOWPF; Bulian et al., 2021); e) the sum of cold eutrophic water planktic foraminifer species (CEWPF; Bulian et al., 2021); f) distribution of benthic Cluster 2D. The shaded rectangles highlight the cycles before and after the restriction event.

limit of ~1200 m (Bandy and Chierici, 1966; Wright, 1978), the estimated depth range is approximately 1000–1500 m for Site 976. *Elphidium* and *Rosalina* spp., discorbids and *Cibicides lobatulus* are present in abundances between 5% and 10% (Fig. 3; Appendix 1) with two maxima of 15% and 20% around 589 m. When found in deep environments, these shallow-water, sometimes epiphytic taxa (Jorissen, 1987; Langer, 1993) are considered displaced (e.g. Murray, 2006) and cannot be used in the paleodepth reconstruction.

After 7.17 Ma high abundances of *O. umbonatus*, *M. pompilioides*, *M. soldanii* and *Karreriella bradyi* indicate that a mesobathyal environment persists after the 7.17 Ma event (Bandy and Chierici, 1966; Wright, 1978 and references therein; Mackensen et al., 1993; Sen Gupta and Machain-Castillo, 1993a; Loubère, 1996; Bornmalm, 1997; Pérez-Asensio et al., 2012a, 2012b; Kaminski et al., 2013).

5.3. Deterioration of deep-water circulation at 7.17 Ma

5.3.1. Environmental changes and aging of deep-water masses

One of the most abundant species in the upper Tortonian-lowermost Messinian (before 7.17 Ma) record is *S. reticulata*, which has been associated with oxic conditions (Gebhardt, 1999; Kouwenhoven et al., 2003), however has also been reported from hypoxic bottom waters (Katz and Thunell, 1984; Denne and Sen Gupta, 1991; Sgarrella and Moncharmont Zei, 1993; Barra et al., 1998). The species is associated with high abundances of *Cibicidoides* species and *P. bulloides*. *Cibicidoides* species are generally considered epifaunal and associated with oligotrophic, well oxygenated waters (e.g. Lutze and Coulbourn, 1984; Corliss and Chen, 1988; Corliss, 1991; Kaiho and Lamolda, 1999). *Cibicidoides kullenbergi* has also been found encrusted on top of substrates (Lutze and Thiel, 1989; Koho et al., 2008) and in high abundances (50%) in a mesotrophic canyon environment (Koho et al., 2008), suggesting it has opportunistic characteristics and can turn to a filter feeding life mode. *Pullenia bulloides* has been associated with areas of elevated productivity (Mackensen et al., 1985; Mackensen et al., 1993). These species (Cluster 1; Figs. 3 and 5) are generally present during the Tortonian and earliest Messinian in other Mediterranean sites (Seidenkrantz et al., 2000; Kouwenhoven et al., 2003; Kouwenhoven et al., 2006; Iaccarino et al., 2008; Di Stefano et al., 2010). Gradual increase of the Shannon diversity between 608.9 and 592 mbsf reflects the entry of several species in the benthic foraminiferal record (Fig. 3; Supp. 1). The BFAR values vary around a mean of ~150 specimens/cm^2/kyr and stay stable through the lowermost Messinian (Fig. 4), suggesting a constant, moderate productivity. The benthic $\delta^{13}C$ values remain high with short term negative excursions (Fig. 6) pointing to an efficiently ventilated water column. A sill efficiently connecting the Mediterranean and Atlantic permitted a significant inflow-outflow, and allowed the

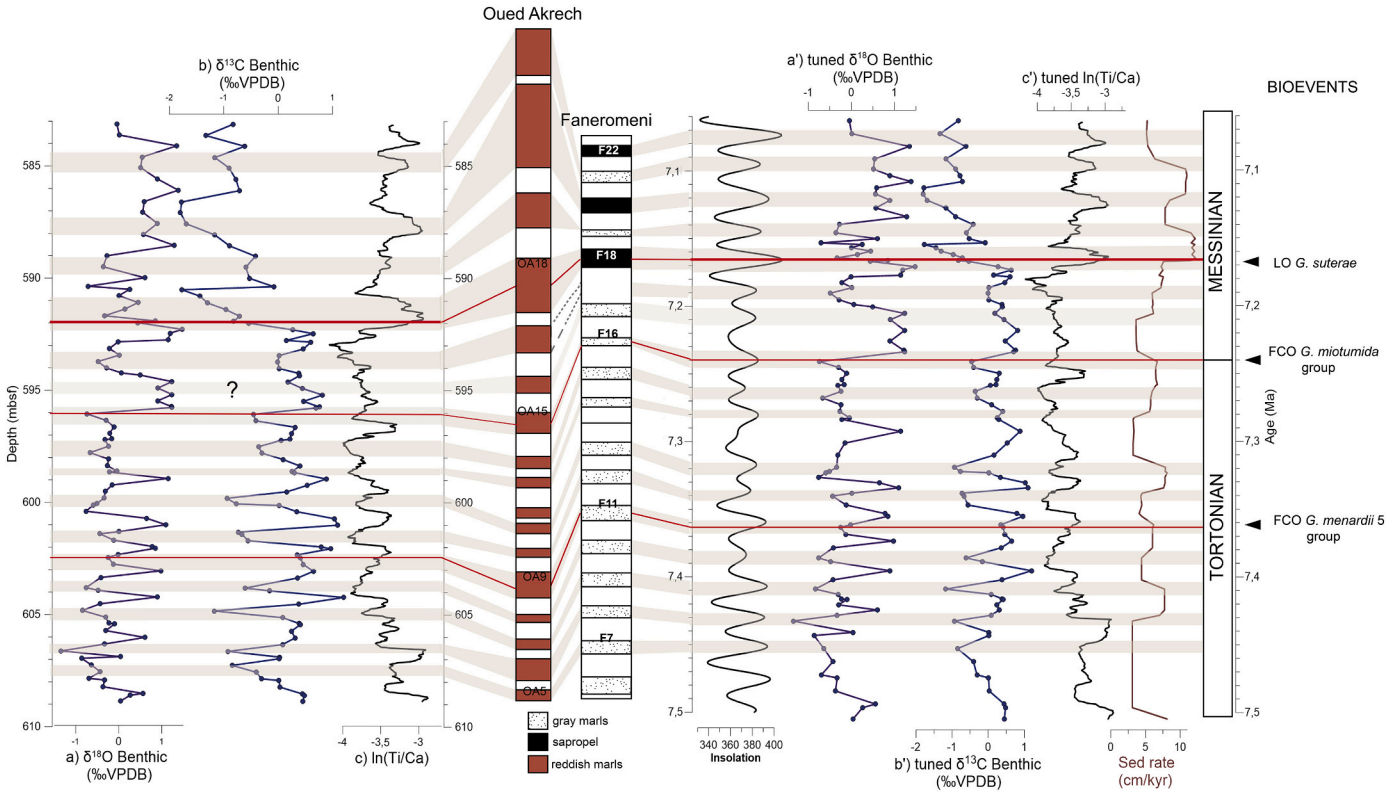

Fig. 10. Age model of ODP Site 976 based on tuning to the insolation curve of the benthic δ18O and δ13C curve and ln(Ti/Ca) ratio. On the left, the records are displayed in depth domain (a, b, c) while on the right in time domain paired with the obtained sedimentation rate (a′, b′, c′). In the Middle, the correlation with the cycles from Oued Akrech (Hilgen et al., 2000) and Faneromeni sections (Krijgsman et al., 1994; Hilgen et al., 1995; Santarelli et al., 1998) is shown. The black arrows show the main foraminifer bioevents (Bulian et al., 2021) highlighted by the red lines. (For interpretation of the references to colour in this figure legend, the reader is referred to the web version of this article.)

Bernoulli aspiration to maintain effective deep water flushing of the seafloor as confirmed by several modeling studies (Alhammoud et al., 2010; Topper and Meijer, 2015). However, the high amplitude oscillations in the benthic $\delta^{13}C$ records suggest that even if deep water renewal was overall effective and prevented sea – floor anoxia in the WMB (values similar as open Atlantic ones; section 5.5), there was a strong precessionally driven variability (around 1‰) suggesting weakened deep water formation during northern hemisphere summer insolation maxima. The $\delta^{13}C$ negative excursions could have been additionally reinforced by deep water admixture with a proto – LIW $\delta^{13}C$ carrying an EMB $\delta^{13}C$ signal (Section 5.4).

The change in the benthic assemblages after 7.17 Ma can be correlated with a similar shift in benthic foraminiferal assemblages occurring at other Mediterranean locations (Seidenkrantz et al., 2000; Kouwenhoven et al., 2003; Kouwenhoven et al., 2006) during deposition of the sapropel astronomically dated by Hilgen et al. (1995) at 7.167 Ma (Section 5.4). The higher abundances of shallow infaunal taxa, tolerating a wide range of conditions and suboptimal oxygen levels (Koho et al., 2008; Kaminski et al., 2013; Cluster 2, Fig. 5) suggests a decrease in bottom-water oxygen levels. According to the TROX model (Trophic-Oxygen: Jorissen et al., 1995), environmental factors predominantly determining species composition of benthic foraminifer assemblages are organic flux and oxygenation of the sea floor; where oxygen levels are more instrumental in establishing the presence or absence of species, whereas quantity and quality (fresh vs degraded) of organic flux structure the communities and determine the relative abundances (Van der Zwaan et al., 1999; Jorissen et al., 2007). This implies that a decrease in bottom-water oxygen and an increase or change of composition of organic flux occurred at the same time, leading to disappearance or decreasing abundances of sensitive species and increasing abundances of more tolerant species. In the WAB, deep infaunal taxa were not dominant at this stage (e.g. *Globobulimina, Chilostomella* spp., *B. aculeata*, *B. dilatata*; Jorissen et al., 2007 and references therein) and anoxic conditions were not reached. Assumptions regarding paleo productivity based on BFAR were not possible for this interval, because the BFAR values lose reliability under reduced oxygen levels (Naidu and Malmgren, 1995). However, a decrease in oxygen levels is also suggested by the rise in S/Ti values. As S can be bound to organic matter (e.g. Lückge et al., 2002), higher S contents in the sediments suggest a higher organic carbon content. Oxidation of organic matter consumes oxygen, therefore a S enrichment suggests an efficient organic matter preservation associated with lowered oxygen levels in the bottom waters (Harff et al., 2011). Further changes in the circulation can be deduced from the $\delta^{13}C$ record of benthic and planktic foraminifers. The sharp drop in the benthic $\delta^{13}C$ record from 0‰ to −1‰ (Fig. 6) and the sharp increase in the $\Delta\delta^{13}C$ to an average value of −2.8‰ imply a prominent increase in residence time of bottom waters in the WAB (Laube-Lenfant and Pierre, 1994).

Coeval with the shift from oxygenated to hypoxic benthic environments, the drop in benthic $\delta^{13}C$ was recorded in other Mediterranean basins suggesting that the 7.17 Ma event had a significant impact on the Mediterranean thermohaline circulation (Section 5.4.2). A shallower strait would mean higher vertical density gradient below the sill depth resulting in a weaker Bernoulli aspiration, inhibiting deep water outflow to the Atlantic. Consequently, deep-water renewal could only be achieved if deep-water formation rates were high enough to result in advection into intermediate water masses. However, in the WAB deep-water formation was not intense enough to incorporate the deeper waters into the MOW, resulting in bottom water aging and oxygen depletion. Surface waters, on the contrary, were less affected (stable planktic $\delta^{13}C$; Fig. 6) possibly because of the proximity of Site 976 to the Mediterranean-Atlantic gateways where the influence of surface-water

inflow carrying the high Atlantic $\delta^{13}C$ signature was stronger. Likewise, while the planktic $\delta^{18}O$ trend is stable, the benthic $\delta^{18}O$ record shows an increasing upward trend suggesting progressively higher bottom water salinities.

5.3.2. Location of the late Tortonian-early Messinian Mediterranean-Atlantic gateway

The Mediterranean scale change in bottom water ventilation excludes the possibility that the WAB was a satellite basin of the Atlantic Ocean and confirms that it was part of the Mediterranean Basin contrary to what was proposed recently. Booth-Rea et al. (2018) suggested that the main gateway restricting the connection between the Mediterranean and the Atlantic during the MSC was located along a volcanic archipelago in the EAB extending southward from the Cabo de Gata region in Southern Spain to the African continent. According to the authors, the emersion of this archipelago would have isolated the WAB from the rest of the Mediterranean and acted as a barrier separating the WAB and the EAB making the WAB an open marine refuge connected with the Atlantic Ocean. This hypothesis was supported by the absence of obvious signs of restriction before 6.8 Ma in previously studied WMB sections like the lower Abad member in the Sorbas basin, where sapropels were only deposited after 6.8 Ma (Sierro et al., 2003). Our new evidence from ODP Site 976 shows that the 7.17 Ma gateway shoaling affected the WAB, confirming that the restriction occurred in the west rather than in the east of the WAB as suggested by Booth-Rea et al. (2018). Hence, we consider that the 7.17 Ma event was triggered by the restriction of the previously defined Gibraltar Arc gateways (see Introduction).

5.4. A Mediterranean scale change in thermohaline circulation: Comparison between the Western and Eastern Mediterranean Basins

With the aim of reconstructing the Mediterranean deep and intermediate circulation before and after the 7.17 Ma gateway restriction event, the Site 976 record has been compared with geochemical, sedimentological and micropaleontological data collected in other Mediterranean sections (Fig. 11 a) including intermediate (300–600 m depth) and deep-water signals (>800 m depth). The depth reconstructions based on foraminifer assemblages and %*P* values reported in literature (Ryan, 1976; Kouwenhoven et al., 1999; e.g. Baggley, 2000; Roger et al., 2000; Fortuin and Krijgsman, 2003; Kouwenhoven et al., 2003; Krijgsman et al., 2006; Hüsing et al., 2009; Di Stefano et al., 2010; Corbí et al., 2020), helped define the intermediate (Sorbas, Bajo Segura, Nijar, Murcia, Melilla, Pissouri Basins and Trave, Monte dei Corvi and Faneromeni sections) and deep basins (Alboran Basin, Balearic promontory, Monte del Casino, Monte Gibliscemi and Metochia sections).

5.4.1. Mediterranean thermohaline circulation until 7.17 Ma

Based on the foraminiferal record, before 7.17 Ma the Western Mediterranean Basin (WMB) was an open marine environment with a well ventilated water column as no sapropels or organic rich layers have been recorded neither in the intermediate basins like Sorbas (Sierro et al., 2003), Nijar (Fortuin and Krijgsman, 2003), Murcia (Krijgsman et al., 2006), Bajo Segura (Corbí et al., 2020) nor in deeper basins such as the Balearic promontory (Ochoa et al., 2015), the Tyrrhenian Sea (Kastens et al., 1988; Glacon et al., 1990) and Alboran Basin. In contrast, sapropels were formed in the Eastern Mediterranean Basin (EMB) during the most prominent insolation maxima. Bottom water anoxia was recorded in deep water sections like Metochia in Greece (Seidenkrantz et al., 2000), the Italian Monte Gibliscemi (Sprovieri et al., 1996; Sprovieri et al., 1999; Blanc-Valleron et al., 2002; Kouwenhoven et al., 2003) and Monte del Casino sections (Krijgsman et al., 1997; Kouwenhoven et al., 2003), and marginal locations like Italian Monte dei Corvi (Hüsing et al., 2009) section. Comparison of the benthic $\delta^{13}C$ from Site 976 (this study) with the Metochia section in the EMB and the Atlantic $\delta^{13}C$ records (Fig. 12), shows that both the EMB and WMB were well ventilated at times of insolation minima, showing high $\delta^{13}C$ values comparable to those recorded at the Atlantic side of the Rifian corridor (e.g. Sale Briqueterie). Still, at times of insolation maxima, a weaker deep water Mediterranean thermohaline circulation probably occurred in both basins. During these times a strong benthic $\delta^{13}C$ depletion was recorded in the WAB (Fig. 12), were values well below the Atlantic ones were found indicating that deep Mediterranean waters immediately to the east of the late Miocene Straits (Betic and Rifian corridors, proto-Gibraltar strait?) were considerably older than the coeval Atlantic water mass. Nonetheless, probably because this area benefited of a local deep – water source like the Gulf of Lions, bottom water anoxia was prevented and lower $\delta^{13}C$ values could reflect the LIW signal from the east. However, these events of anoxia were not registered in the benthic $\delta^{13}C$ record (see the Metochia record in Fig. 12) because isotope analyses were only carried out in the non – sapropelic samples. Even though the Mediterranean-Atlantic connection was wide open, the presence of sapropels in the EMB suggests a less efficient deep/intermediate water circulation than in the WMB. This discrepancy can be explained by the weaker Bernoulli aspiration at the Sicily sill (Rohling et al., 2015) that would block the incorporation of part of the deep water in the outflow to the WMB, preventing an efficient ventilation of the bottom (Fig. 11 b).

5.4.2. Mediterranean thermohaline circulation after 7.17 Ma

With a shallowing of 120 m at the Strait of Gibraltar (Myers et al., 1998; Rohling et al., 2015) assumed for the for the last glacial maximum, salinities above 40 psu have been modelled for the Mediterranean. Similarly at 7.17 Ma, the reduced water exchange with the Atlantic led not only to a longer bottom water residence time but possibly to higher bottom water salinities (e.g. Meijer, 2006). With a shallower strait, the Bernoulli aspiration depth would reduce, producing progressively saltier and higher density deep waters increasing the density contrast between what was left of the Atlantic inflow and Mediterranean deep – water masses, favouring water – mass stratification (as shown by models, e.g. Meijer, 2006), a less efficient deep water circulation and consequently increased bottom water residence time (e.g. Sierro et al., 2003). Under this regime and at smaller time scales, precession forced cyclical changes in the hydrological budget would, during periods of enhanced freshwater discharge, further enhance stratification leaving a stronger impact on the Mediterranean circulation (Simon et al., 2017).

At Site 976, deterioration of the deep circulation at 7.17 Ma is visible from the sharp drop in benthic $\delta^{13}C$ and the shift towards more hypoxic benthic foraminifer associations, while water column stratification is indicated by the first appearance of the warm water planktonic foraminifer genus *Globigerinoides* (Bulian et al., 2021) and by the sharp $\Delta\delta^{13}C$ gradient. From 7.17 Ma onward, similar changes have been recorded at several WMB shallow marginal basins. In the Bajo Segura (Corbí et al., 2020) and Murcia (Krijgsman et al., 2006) basins an increase of benthic stress taxa has been reported, suggesting a moderate reduction in deep – water ventilation while the beginning of cyclical deposition of diatomite rich layers in the Nijar (Fortuin and Krijgsman, 2003) and Sorbas (Sierro et al., 2003) basins suggest higher sensitivity towards precessionally induced climate variability (Fig. 11 c). Yet, the deep WMB water never reached anoxia as sapropels do not occur in the marginal basins until the second restriction step at 6.8–6.7 Ma, when the first sapropels are identified at the base of the Upper Abad member (Sierro et al., 2001; Sierro et al., 2003) in the Sorbas and Nijar basins. The WAB surface waters, in addition, were not affected by the restriction (e.g. Sorbas Basin-Sierro et al., 2003 and this study), suggesting the presence of an Atlantic inflow with the typical high planktic $\delta^{13}C$ of the open ocean. One exception in the WMB is the Tyrrhenian basin as the sedimentological record of ODP Site 654 shows, starting around 7.2 Ma, deposition of dolomitic dark shales characterized by extremely rare or absent foraminifers (Glacon et al., 1990) suggesting the installation of an anoxic bottom environment. However, Roveri et al. (2014b) and Borsetti et al. (1990) suggest that these sediments are actually much younger and that hiatus explains this anomaly. In the EMB on the other hand, oxygen depleted conditions are visible from the onset of euxinic shale and

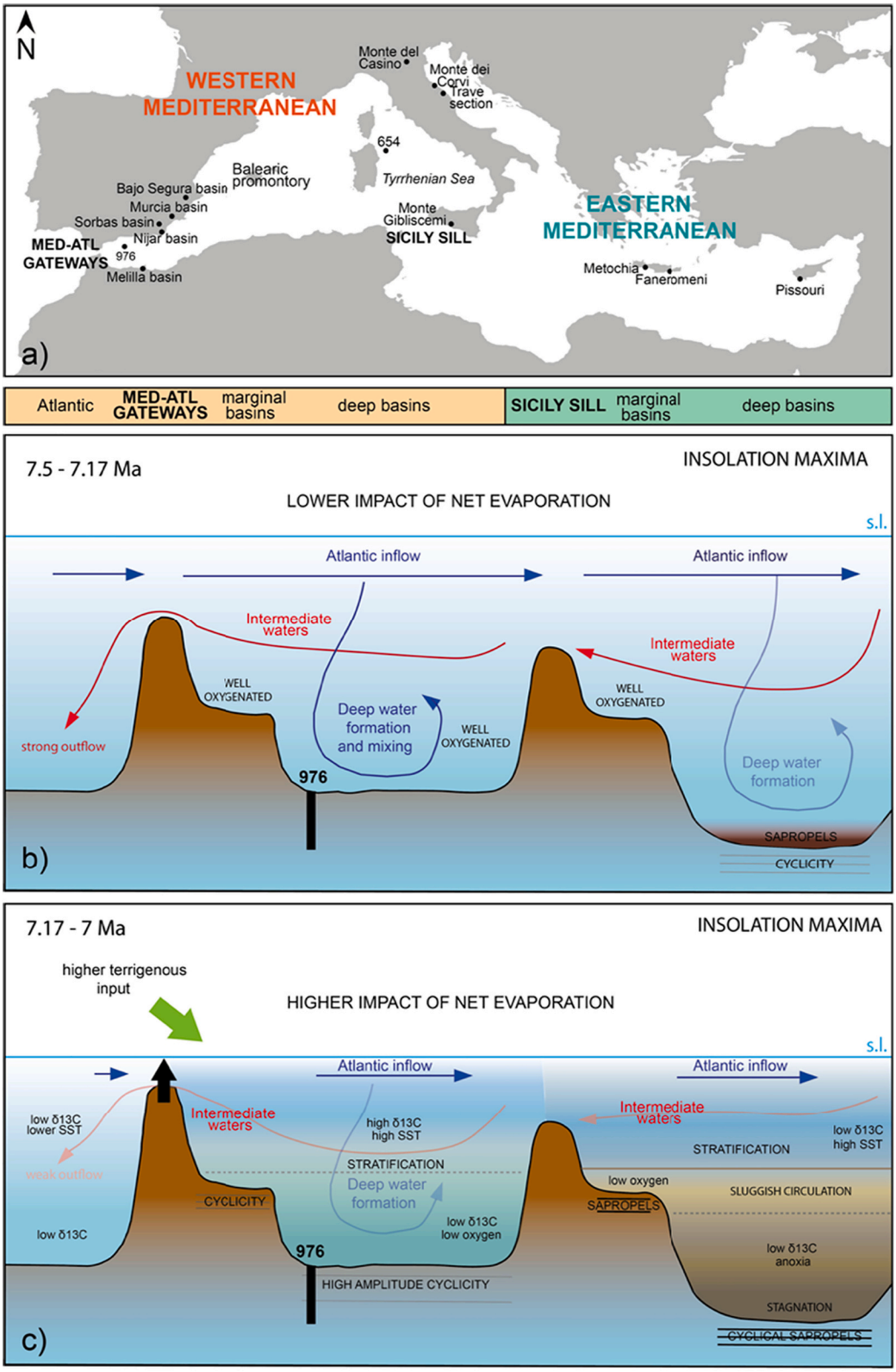

Fig. 11. a) Generalized map of the Mediterranean Sea showing the basins, sections and ODP Sites mentioned in this section. Cartoon showing the Mediterranean thermohaline circulation: b) before (from present circulation studies like Pinardi and Masetti, 2000) and c) after the 7.17 Ma event. Circulation patterns adapted from (Alhammoud et al., 2010) and (Topper and Meijer, 2015).

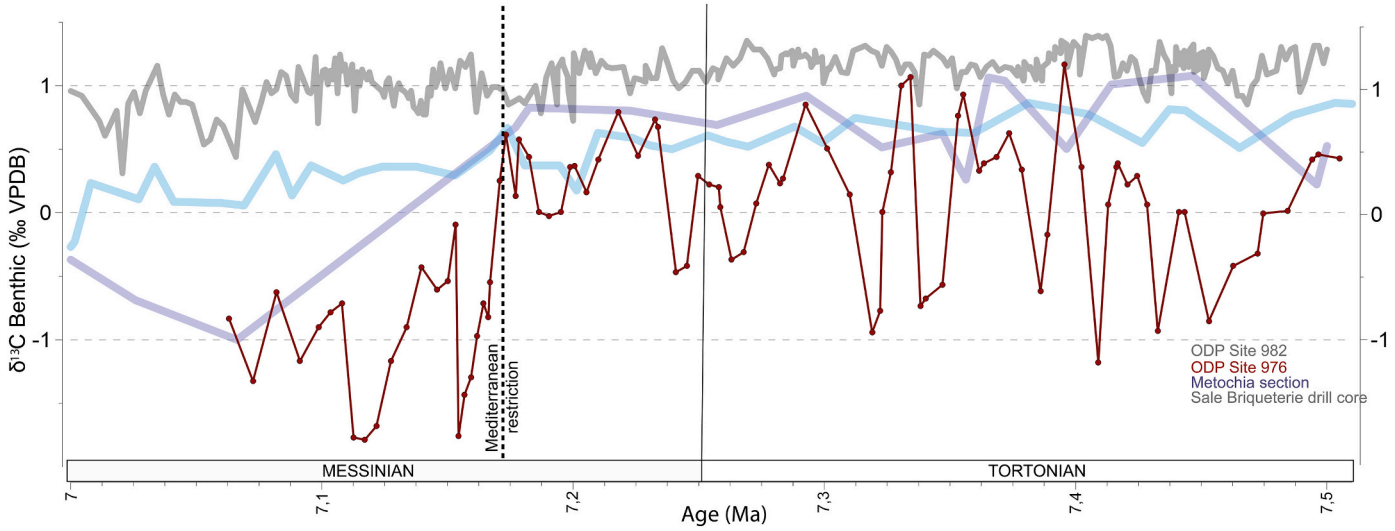

Fig. 12. Comparison between benthic δ13C records of Site 976 in red (this study), Atlantic Ocean ODP Site 982 (Drury et al., 2018) in grey, Metochia section (Seidenkrantz et al., 2000) in purple, and Atlantic drill site Sale Briqueterie (Hodell et al., 1994) in light blue. In order to compare the absolute values of the curves, the isotope records that were measured on different benthic foraminifera species than Site 976 were corrected according to their offset with respect to *Cibicides kullenbergi* reported in literature. Metochia and Sale Briqueterie records were obtained from *Planulina ariminensis*. The correction of the offset with respect to *C. kullenbergi* was obtained using the correction factors from Van der Laan et al. (2006), where isotope analyses performed on samples from the Loulja section (Morocco) both on *C. pachyderma* and *P. ariminensis* showed an interspecific offset of 0.627‰ for δ13C measurements. The isotopic record ofSite 982 ODP, measured on *C. wuellerstorfi* or *C. mundulus* did not need any correction because no offset has been found between the two species (Hodell et al., 2001; Holbourn et al., 2007; Holbourn et al., 2018). The continuous black line highlights the Tortonian – Messinian boundary while the dashed one the 7.17 Ma restriction event. (For interpretation of the references to colour in this figure legend, the reader is referred to the web version of this article.)

sapropel deposition in the marginal Monte dei Corvi (Hüsing et al., 2009) and Faneromeni sections (Santarelli et al., 1998), together with more frequent sapropels in deep locations like Metochia and Monte del Casino sections (Kouwenhoven et al., 1999; Seidenkrantz et al., 2000). In the EMB, the abrupt $\delta^{13}C$ decrease in benthic (Fig. 12) and planktic records (e.g. Metochia section: Seidenkrantz et al., 2000; Monte Gibliscemi: Sprovieri et al., 1996; Monte del Casino: Kouwenhoven et al., 2003 and Faneromeni section: Kontakiotis et al., 2019) suggest that significant increase in residence time affected both deep and intermediate water cells. At the same time, a trend towards heavier values of both planktic and benthic $\delta^{18}O$ curves from Metochia and Monte del Casino sections possibly indicate higher bottom water salinities (Kouwenhoven et al., 2003).Planktic species indicating stressful conditions (*Turborotalita quinqueloba, Globigerinita glutinata, Globigerinella obesa, Orbulina universa*) (Seidenkrantz et al., 2000; Kouwenhoven et al., 2006; Di Stefano et al., 2010) together with benthic species implying limited oxygen levels and increased salinities become more abundant in the marginal basins, while deep basins show low diversity benthic foraminifer assemblages, often dominated by bolivinids (e.g. Seidenkrantz et al., 2000). The proliferation of this benthic species can be attributed to increased salinities and reduced oxygen levels, changes conformable with a gateway restriction scenario.

From 7.17 Ma onward, the restriction of the Mediterranean-Atlantic gateway/s and reduction of water exchange between the two basins, paired with the negative Mediterranean freshwater budget resulted in a change in the thermohaline circulation that impacted to different extents the WAB and EMB. Higher density contrast between WMB deep – water masses and inflowing Atlantic surface waters resulted in increasing vertical density gradients leading to water column stratification. Here, close to the gateway, surface waters were able to preserve the Atlantic isotopic signal while deep waters show clear signs of aging and decreasing oxygen levels. These effects are linked with aspiration depth reduction (i.e., Bernoulli aspiration) at the Gibraltar gateway/s which limited water outflow and with less deep – water formation in the Gulf of Lions related to presence of dense Levantine intermediate water from the East, which could not mix with the much fresher Atlantic water given the too high density contrast. More pronounced effects have been recorded in the EMB. It is likely that the presence of the Sicily sill with even lower aspiration depth hindered, for the larger part, the escape of deep waters from the EMB towards the WMB, resulting in aged, anoxic, and stagnant bottom waters with sapropel deposition during insolation maxima. Longer water residence time has been registered in EMB surface waters as well. Here, far from the Atlantic Ocean, surface waters could reflect the deep-water signal. In particular, the different configuration of the WMB and EMB and consequent non identical reaction to circulation changes have been noticed also in the Plio-Quaternary Mediterranean records, where during insolation maxima sapropels form only in the EMB, while in the WMB bottom waters never reach anoxia but only enrichment in organic matter that allows the development of ORLs (e.g. Murat, 1999; Rogerson et al., 2008). This suggests that from 7.17 Ma onward, the configuration of the Mediterranean Basin was very similar to the recent one. Nonetheless, to better understand the Mediterranean-Atlantic connectivity and circulation prior to this event late Miocene continuous records from other deep WMB are needed.

5.5. Correlation of the Mediterranean restriction and LMCIS

During the Late Miocene cooling (7.5–5.5 Ma) a global decrease in sea surface temperatures (SST) of about 6 °C (compared to the mean present day SST) has been reconstructed (Herbert et al., 2016) contemporaneously with a global decrease in $\delta^{13}C$ oceanic values (Fig. 13 a and b) related with the LMCIS (7.8–6.7 Ma; Hodell et al., 1994; Hodell et al., 2001; Hodell and Venz-Curtis, 2006). During this period of time of 1.1 Ma, the amplitude of the $\delta^{13}C$ decrease reached 0.75‰ in the Atlantic and 1‰ in the Pacific ocean which is visible for example in Atlantic ODP sites 982 (Hodell et al., 2001; Drury et al., 2018), 926 (Drury et al., 2017), the Salé Briqueterie core (Hodell et al., 1994) and China Sea ODP Site 1146 (Holbourn et al., 2018; Holbourn et al., 2021). In this work we will focus only on the final stage of the LMCIS (7.2 Ma – 6.8 Ma) part of which is recorded at Site 976 (Fig. 13 b). Over the final 0.4 Ma of the LMCIS, in the Atlantic sites the $\delta^{13}C$ dropped with 0.30–0.35‰, while in the South China Sea a more pronounced drop of

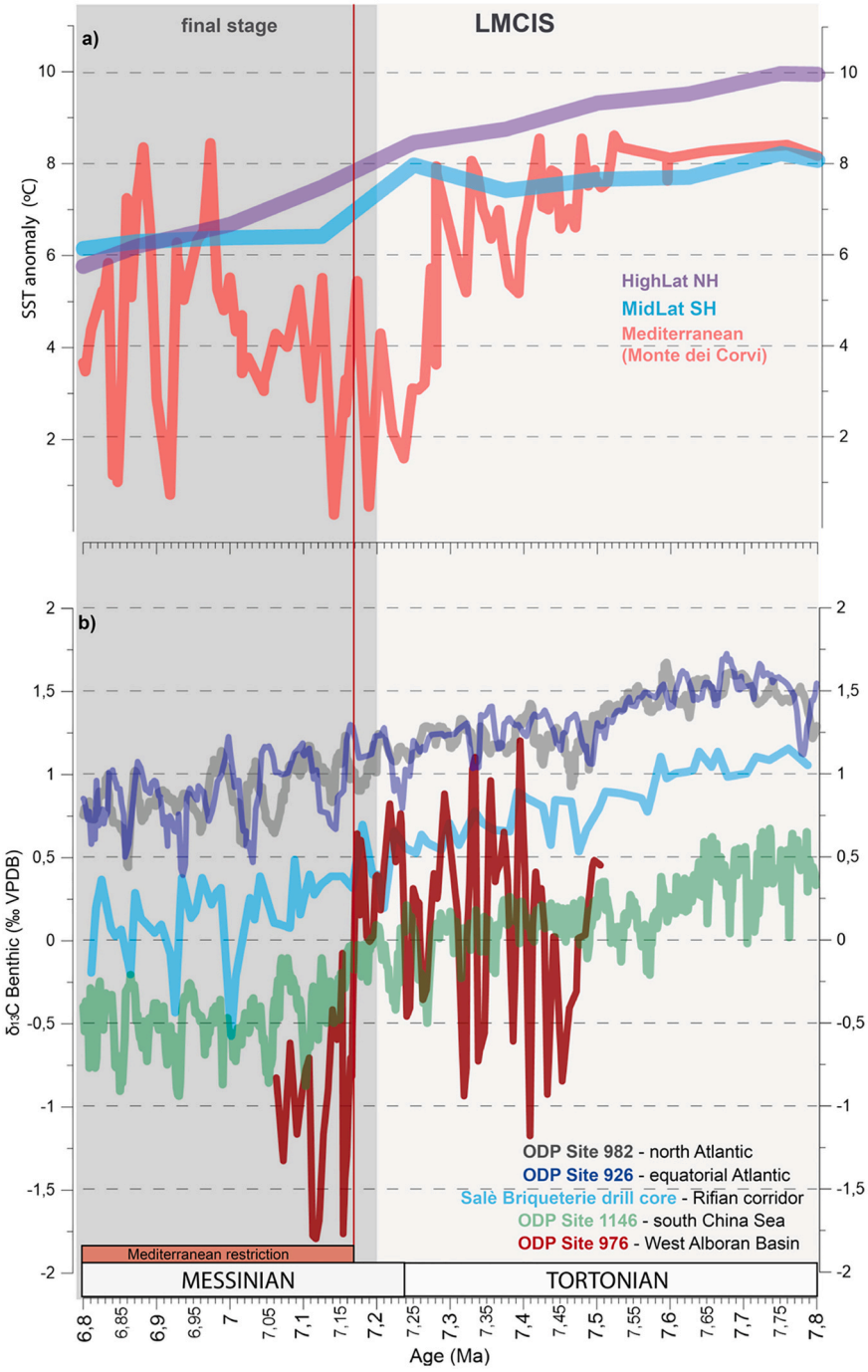

Fig. 13. a) Sea surface temperatures (SST) for Northern Hemisphere high-latitudes, Southern Hemisphere mid-latitudes (Herbert et al., 2016) and Mediterranean Sea (Monte dei Corvi section, Italy; Tzanova et al., 2015); b) Comparison between benthic δ13C records of ODP Site 976 in red (this study), Atlantic ODP Site 982 in grey (Drury et al., 2018), Equatorial Atlantic ODP Site 926 in dark blue (Drury et al., 2017), Salé Briqueterie drill core in light blue (Hodell et al., 1994), and South China Sea ODP 1146 Site in green (Holbourn et al., 2018; Holbourn et al., 2021). In order to compare the absolute values of the curves, the isotope records that were measured on other benthic foraminifera species than for Site 976 were corrected according to their offset with respect to *Cibicides kullenbergi* reported in literature. The Sale Briqueterie record was obtained from *Planulina ariminensis* and to correct its offset the correction factors were taken from Van der Laan et al. (2006, Loulja section, Morocco), where δ13C analyses performed both on *C. pachyderma* (should yield equivalent values as *C. kullenbergi*; Riveiros et al., 2010) and *P. ariminensis* showed an interspecific offset of 0.627‰. When the isotopic record was obtained measuring *C. wuellerstorfi* or *C. mundulus* (ODP sites 982, 1146 and 926) no correction has been applied because no offset has been found between the three species (Hodell et al., 2001; Holbourn et al., 2007; Holbourn et al., 2018). Light grey shading marks the LMCIS while the dark grey shading its final stages. (For interpretation of the references to colour in this figure legend, the reader is referred to the web version of this article.)

~0.75‰, (Holbourn et al., 2018) has been registered. At Site 976, the amplitude of the $\delta^{13}C$ drop (~1‰), which occurred at exactly 7.17 Ma coinciding with the major restriction event, is even higher (Fig. 13 b) and is clearly more abrupt when compared with the more gradual change observed in the open Ocean. However, at Site 1146, the most significant decrease in benthic $\delta^{13}C$ the LMCIS occurred between 7.2 and 7 Ma (Holbourn et al., 2018) making it almost coeval with the 7.17 Ma event (Fig. 13 b). A detailed comparison between the two benthic $\delta^{13}C$ records, however, reveals different responses of the two systems (Fig. 14). The benthic $\delta^{13}C$ from ODP Site 1146 follows a global pattern of lower benthic $\delta^{13}C$ at glacial periods with larger ice volume (higher benthic $\delta^{18}O$) during obliquity minima probably due to a greater CO_2 storage in the deep ocean (Holbourn et al., 2018). By contrast, the Mediterranean benthic $\delta^{13}C$ cyclicity is controlled by northern hemisphere summer insolation and lower benthic $\delta^{13}C$ values are recorded during insolation maxima. This implies that, while open ocean stable isotope signals are dominated by obliquity, the Mediterranean Sea record is modulated by precession. According to our age model (Fig. 10), the two pronounced drops in $\delta^{13}C$ recorded at Site 976 after 7.17 Ma (590.5 and 587 mbsf) show higher amplitudes because they occurred during a period of interference between obliquity and precession (when the two curves are in phase), when changes in freshwater budget are amplified. The latter can be correlated to the first and second prominent sapropels (Fig. 14: black layers at 34.5 and 37 m) in the Faneromeni section in the EMB (cycles F18-F22; Krijgsman et al., 1994; Hilgen et al., 1995; Santarelli et al., 1998), while smaller changes in the $\delta^{13}C$ record are linked to low amplitude peaks in summer insolation during obliquity minima resulting in the deposition of grey marls instead of sapropels

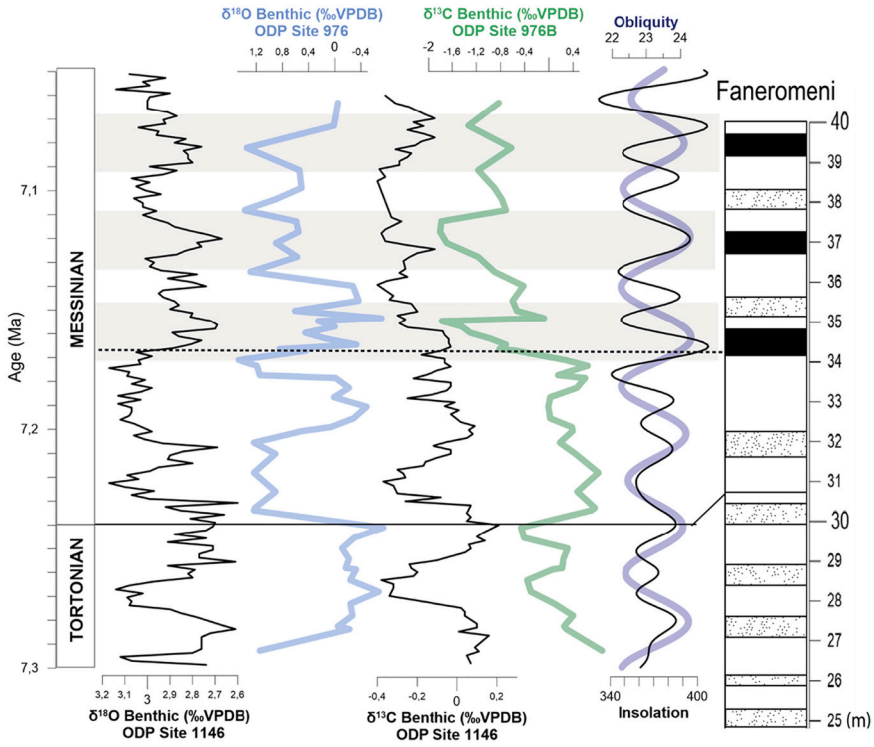

Fig. 14. The benthic $\delta^{18}O$ and $\delta^{13}C$ curves from China Sea ODP 1146 Site (Holbourn et al., 2018; Holbourn et al., 2021) and WAB ODP 976 Site are shown followed by the obliquity curve by Laskar et al. (2004). The grey shadings highlight obliquity maxima phases and correlate them with sapropel deposition in Faneromeni section (Krijgsman et al., 1994; Hilgen et al., 1995; Santarelli et al., 1998). The continuous black line highlights the Tortonian – Messinian boundary while the dashed one the 7.17 Ma restriction event.

(35.5 and 38 m; Santarelli et al., 1998). In a highly restricted basin with elevated bottom – water salinities like the Mediterranean, the increase in precipitation that characterizes summer insolation maxima would result in high amounts of low-density freshwaters, promoting strong water stratification. Under these circumstances deep – water formation would not be possible and therefore deep – water renewal would be blocked resulting in an increased residence time of deep water with subsequent lowering of the $\delta^{13}C$. The lower CO_2 levels (Zhang et al., 2013; Tanner et al., 2020) that characterize the LMCIS have also been linked to a global increase in ice volume (Drury et al., 2016; Herbert et al., 2016). In a context of tectonic uplift that progressively reduced the section of the Mediterranean – Atlantic straits, a sea level drop associated with ice volume expansion during the LMCIS could have further reduced the water exchange with the Atlantic and amplified the drop in benthic $\delta^{13}C$. This could explain why the South China Sea continued to reflect a global signal while the stronger isolation of the Mediterranean from the Global Ocean made it more sensitive to local hydrological budget changes.

The global cooling during the LMCIS (Herbert et al., 2016) seems to be recorded in the Mediterranean Monte dei Corvi section where the SST underwent a sudden drop (Fig. 13 a) of ~6 °C dated at 7.25 Ma (Tzanova et al., 2015). Apart from an overall SST decrease, SST values are lower at times of vertical mixing during insolation minima and higher at times of strong stratification of the water column during sapropel formation (Tzanova et al., 2015). The lowest temperatures in Monte del Corvi occur during an interval in the earliest Messinian without sapropel formation (Tzanova et al., 2015) suggesting vertical mixing was permanent during this time. Cooling in northern Europe and the influence of northern winter winds, similar to the Bora winds today (Boldrin et al., 2009 and references therein), may have lowered the SST and favoured mixing of the water column during this period. Winter mixing would have increased nutrient content at the surface stimulating phytoplankton productivity and alkenone production. Contrary to the Adriatic, the WAB registers vertical mixing before 7.17 Ma and more stratification after this event probably due to the southern position of the Alboran Basin, far from the influence of the northern cool winds. Indeed, today the southern margin of the Mediterranean is more prone to water stratification favouring the growth of warmer-water planktonic foraminifer species (Azibeiro et al., in prep) where the stratification is only broken in the northern coast of the Alboran Sea due to the upwelling cells associated with the anticyclonic gyres. This explains the continuous dominance of cold-water species before 7.17 Ma in the Alboran Basin when a more intense exchange resulted in higher upwelling intensities. The lower Atlantic Mediterranean exchange after 7.17 Ma reduced the upward advection of cold water, favouring stratification that reduced the proportion of cold – water species and increased the warm oligotrophic, especially at times of insolation maxima. This argues in favour of water stratification and the subsequent surface warming as the main cause of the higher proportion of warm water species in the WAB, implying that the restriction of the Mediterranean-Atlantic gateways was the main force influencing Mediterranean circulation after 7.17 Ma, while the cooling visible in Monte dei Corvi section can be a localized event.

6. Conclusions

The integrated upper Tortonian-lower Messinian micropaleontological and geochemical data of ODP Site 976 in the West Alboran Basin (WAB) presented in this study improved the age control based on cyclostratigraphy. Using as tie points planktic foraminifer bio events in combination with new stable isotope and elemental records allowed the creation of a new improved age model. This enabled a more detailed correlation with other Mediterranean records and confirmed that the gateway restriction starting from 7.17 Ma changed the WAB marine environments at the same time it affected different locations all over the basin, suggesting a Mediterranean-scale change in thermohaline circulation. From these data follows that the WAB and EAB were not separated by a sill, which would render the WAB a satellite basin of the Atlantic, but that the WAB was part of the Mediterranean realm.

Until 7.17 Ma, the WAB represented a deep-water well-ventilated environment, indicating efficient water exchange through the Gibraltar gateway/s. Starting from 7.17 Ma, the intense uplift of the Gibraltar Arc caused the progressive closure of the Betic and Rifian corridors and a

diminished connection with the Global Ocean. This paleogeographic reorganization impacted the deeper part of the WAB as reflected by the benthic foraminiferal fauna, which became dominated by shallow infaunal taxa, tolerant to a wide range of conditions and suboptimal oxygen levels. These observations, paired with a significant drop in benthic $\delta^{13}C$ values suggests that the progressive Mediterranean-Atlantic gateway restriction led to the decrease in bottom water oxygen levels and increase in its residence time.

The correlation between Site 976 and previously published data, enabled to refine models of the Mediterranean circulation before and after 7.17 Ma. The restriction of the gateways resulted in stratification of the WMB water column and showed that while the bottom waters were depleted in oxygen, the intermediate waters were better ventilated. This evaluation also confirmed that, because of the presence of the Sicily sill, the impact of stratification was much higher in the EMB where it led to sapropel deposition, absent in the WMB.

The paleoenvironmental change at 7.17 Ma coincided with the LMCIS (7.6 to 6.8/7 Ma), a global event characterized by cooling and a shift to lighter $\delta^{13}C$. In particular, the correlation of the isotope data of Site 976 with those of ODP Site 1146 in the South China Sea showed that both basins register a larger and more instantaneous $\delta^{13}C$ shift. However, the phase relations of the isotope record with astronomical parameters (precession, obliquity) are different. Site 1146 reflects global phase relations connected to glacial stages, whereas the phase relations in the WAB depend on hydrological budget changes suggesting a much stronger local effect in the Mediterranean. Considering that the LMCIS has been related to ice volume expansion, the gateway restriction effects on the Mediterranean could have been further amplified by a relative sea level drop.

Credit author statement

Francesca Bulian: conceptualization, investigation, methodology, sample preparation (foraminifers, stable isotopes, element analysis), data acquisition, data analysis, interpretation, writing - original draft preparation. **Tanja Kouwenhoven**: benthic foraminifers: methodology, data analysis, supervision, interpretation, writing - reviewing and editing. **Francisco J. Jiménez-Espejo**: element analysis, data analysis, interpretation, writing - reviewing and editing. **Nils Andersen**: stable isotope analysis (planktic and benthic foraminifers), reviewing and editing. **Wout Krijgsman**: resources, conceptualization, supervision, writing - reviewing and editing. **Francisco J. Sierro**: resources, conceptualization, supervision, interpretation, writing - reviewing and editing, sample curation.

Data statement

All data used in this study are available in the public repository Mendeley Data as: Bulian, Francesca; Sierro, Francisco J.; Kouwenhoven, Tanja J.; Andersen, Nils (2021), "Geochemical and micropaleontological analyses from ODP Site 976B (Leg 161) in the West Alboran Basin", Mendeley Data, V3, doi: 10.17632/ggpmmxr8k3.3.

Declaration of Competing Interest

The authors declare that they have no conflict of interest, neither financial nor personal that could have appeared to influence the work reported in this paper.

Acknowledgments

The authors appreciate the work of Jose Ignacio Martin Cruz in sample processing and preparation. Furthermore, all fellow ESRs and supervisors from the SALTGIANT project are thanked for their valuable suggestions and discussions. Two anonymous reviewers are gratefully acknowledged for critical reading and detailed comments which were very helpful to improve the original manuscript. This research used data and samples collected through ODP Expedition 161 aboard the Joides Resolution. Geochemical data was acquired at the XRF Core Scanner Lab at the MARUM – Center for Marine Environmental Sciences, University of Bremen, Germany. This research has received funding from the European Union's Horizon 2020 research and innovation program under the Marie Skłodowska-Curie grant agreement n° 765256 SALTGIANT.

Appendix A. Supplementary data

Supplementary data to this article can be found online at https://doi.org/10.1016/j.palaeo.2022.110841.

References

Achalhi, M., Münch, P., Cornée, J.-J., Azdimousa, A., Melinte-Dobrinescu, M., Quillévéré, F., Drinia, H., Fauquette, S., Jiménez-Moreno, G., Merzeraud, G., Moussa, A.B., El Kharim, Y., Feddi, N., 2016. The late Miocene Mediterranean-Atlantic connections through the North Rifian Corridor: New insights from the Boudinar and Arbaa Taourirt basins (northeastern Rif, Morocco). Palaeogeogr. Palaeoclimatol. Palaeoecol. 459, 131–152.

Alhammoud, B., Meijer, P.T., Dijkstra, H.A., 2010. Sensitivity of Mediterranean thermohaline circulation to gateway depth: a model investigation. Paleoceanography 25 (2).

Baggley, K.A., 2000. The late tortonian-early Messinian foraminiferal record of the Abad Member (Turre Formation), Sorbas Basin, Almería, South-East Spain. Palaeontology 43 (6), 1069–1112.

Bahr, A., Lamy, F., Arz, H., Kuhlmann, H., Wefer, G., 2005. Late glacial to Holocene climate and sedimentation history in the NW Black Sea. Mar. Geol. 214 (4), 309–322.

Bandy, O.L., Chierici, M.A., 1966. Depth-temperature evaluation of selected California and Mediterranean bathyal foraminifera. Mar. Geol. 4 (4), 259–271.

Barra, D., Bonaduce, G., Sgarrella, E., 1998. Paleoenvironmental bottom water conditions in the early Zanclean of the Capo Rossello area (Agrigento, Sicily). Bollettino-Soc. Paleontol. Italiana 37, 61–88.

Bianchi, D., Zavatarelli, M., Pinardi, N., Capozzi, R., Capotondi, L., Corselli, C., Masina, S., 2006. Simulations of ecosystem response during the sapropel S1 deposition event. Palaeogeogr. Palaeoclimatol. Palaeoecol. 235 (1–3), 265–287.

Blanc-Valleron, M.-M., Pierre, C., Caulet, J., Caruso, A., Rouchy, J.-M., Cespuglio, G., Sprovieri, R., Pestrea, S., Di Stefano, E., 2002. Sedimentary, stable isotope and micropaleontological records of paleoceanographic change in the Messinian Tripoli Formation (Sicily, Italy). Palaeogeogr. Palaeoclimatol. Palaeoecol. 185 (3–4), 255–286.

Blondel, C., Merceron, G., Andossa, L., Taisso, M.H., Vignaud, P., Brunet, M., 2010. Dental mesowear analysis of the late Miocene Bovidae from Toros-Menalla (Chad) and early hominid habitats in Central Africa. Palaeogeogr. Palaeoclimatol. Palaeoecol. 292 (1–2), 184–191.

Boldrin, A., Carniel, S., Giani, M., Marini, M., Aubry, F.B., Campanelli, A., Grilli, F., Russo, A., 2009. Effects of bora wind on physical and biogeochemical properties of stratified waters in the northern Adriatic. J. Geophys. Res. Oceans 114 (C8).

Booth-Rea, G., Ranero, C.R., Grevemeyer, I., 2018. The Alboran volcanic-arc modulated the Messinian faunal exchange and salinity crisis. Sci. Rep. 8 (1), 13015.

Bornmalm, L., 1997. Taxonomy and paleoecology of late Neogene benthic foraminifera from the Caribbean Sea and eastern equatorial Pacific Ocean. Fossils and Strata No. 41, pp. 1–96.

Borsetti, A., Curzi, P., Landuzzi, V., Mutti, M., Lucchi, F.R., Sartori, R., Tomadin, L., Zuffa, G., 1990. Messinian and pre-Messinian sediments from ODP Leg 107 sites 652 and 654 in the Tyrrhenian Sea: sedimentologic and petrographic study and possible comparisons with italian sequences. Proc. ODP, Sci. Results 107, 169–186.

Bosmans, J., Drijfhout, S., Tuenter, E., Hilgen, F., Lourens, L.J., Rohling, E., 2015. Precession and obliquity forcing of the freshwater budget over the Mediterranean. Quat. Sci. Rev. 123, 16–30.

Bulian, F., Sierro, F.J., Ledesma, S., Jiménez-Espejo, F.J., Bassetti, M.-A., 2021. Messinian West Alboran Sea record in the proximity of Gibraltar: early signs of Atlantic-Mediterranean gateway restriction. Mar. Geol. 106430.

Buongiorno Nardelli, B., Salusti, E., 2000. On dense water formation criteria and their application to the Mediterranean Sea. Deep-Sea Res. I Oceanogr. Res. Pap. 47 (2), 193–221.

Calvert, S., Pedersen, T., 2007. Chapter fourteen elemental proxies for palaeoclimatic and palaeoceanographic variability in marine sediments: interpretation and application. Develop. Marine Geol. 1, 567–644.

Capella, W., Barhoun, N., Flecker, R., Hilgen, F., Kouwenhoven, T., Matenco, L., Sierro, F. J., Tulbure, M., Yousfi, M.Z., Krijgsman, W., 2018. Palaeogeographic evolution of the late Miocene Rifian Corridor (Morocco): reconstructions from surface and subsurface data. Earth Sci. Rev. 180, 37–59.

Capella, W., Spakman, W., van Hinsbergen, D.J., Chertova, M.V., Krijgsman, W., 2020. Mantle resistance against Gibraltar slab dragging as a key cause of the Messinian Salinity Crisis. Terra Nova 32 (2), 141–150.

Comas, M.C., Zahn, R., Klaus, A., et al., 1996. ODP, Init. Repts., 161: College Station, TX (Ocean Drilling Program).

Corbí, H., Lancis, C., García-García, F., Pina, J.-A., Soria, J.M., Tent-Manclús, J.E., Viseras, C., 2012. Updating the marine biostratigraphy of the Granada Basin (central

Betic Cordillera). Insight for the Late Miocene palaeogeographic evolution of the Atlantic–Mediterranean seaway. Geobios 45 (3), 249–263.
Corbí, H., Soria, J.M., Giannetti, A., Yébenes, A., 2020. The step-by-step restriction of the Mediterranean (start, amplification, and consolidation phases) preceding the Messinian Salinity Crisis (climax phase) in the Bajo Segura basin. Geo-Mar. Lett. 40 (3), 1–21.
Corliss, B.H., 1991. Morphology and microhabitat preferences of benthic foraminifera from the Northwest Atlantic Ocean. Mar. Micropaleontol. 17 (3–4), 195–236.
Corliss, B.H., Chen, C., 1988. Morphotype patterns of Norwegian Sea deep-sea benthic foraminifera and ecological implications. Geology 16 (8), 716–719.
De Visser, J., Ebbing, J., Gudjonsson, L., Hilgen, F., Jorissen, F., Verhallen, P., Zevenboom, D., 1989. The origin of rhythmic bedding in the Pliocene Trubi Formation of Sicily, southern Italy. Palaeogeogr. Palaeoclimatol. Palaeoecol. 69, 45–66.
Denne, R.A., Sen Gupta, B.K., 1991. Association of bathyal foraminifera with water masses in the northwestern Gulf of Mexico. Mar. Micropaleontol. 17 (3–4), 173–193.
Di Stefano, A., Verducci, M., Lirer, F., Ferraro, L., Iaccarino, S.M., Hüsing, S.K., Hilgen, F. J., 2010. Paleoenvironmental conditions preceding the Messinian Salinity Crisis in the Central Mediterranean: integrated data from the Upper Miocene Trave section (Italy). Palaeogeogr. Palaeoclimatol. Palaeoecol. 297 (1), 37–53.
Drury, A.J., John, C.M., Shevenell, A.E., 2016. Evaluating climatic response to external radiative forcing during the late Miocene to early Pliocene: New perspectives from eastern equatorial Pacific (IODP U1338) and North Atlantic (ODP 982) locations. Paleoceanography 31 (1), 167–184.
Drury, A.J., Westerhold, T., Frederichs, T., Tian, J., Wilkens, R., Channell, J.E., Evans, H., John, C.M., Lyle, M., Röhl, U., 2017. Late Miocene climate and time scale reconciliation: Accurate orbital calibration from a deep-sea perspective. Earth Planet. Sci. Lett. 475, 254–266.
Drury, A.J., Westerhold, T., Hodell, D., Röhl, U., 2018. Reinforcing the North Atlantic backbone: revision and extension of the composite splice at ODP Site 982. Clim. Past 14 (3), 321–338.
Edwards, E.J., Osborne, C.P., Strömberg, C.A., Smith, S.A., Consortium, C.G, 2010. The origins of C4 grasslands: integrating evolutionary and ecosystem science. Science 328 (5978), 587–591.
Emeis, K., Weissert, H., 2009. Tethyan–Mediterranean organic carbon-rich sediments from Mesozoic black shales to sapropels. Sedimentology 56 (1), 247–266.
Fentimen, R., Lim, A., Rüggeberg, A., Wheeler, A.J., Van Rooij, D., Foubert, A., 2020. Impact of bottom water currents on benthic foraminiferal assemblages in a cold-water coral environment: the Moira Mounds (NE Atlantic). Mar. Micropaleontol. 154, 101799.
Flecker, R., Krijgsman, W., Capella, W., De Castro Martíns, C., Dmitrieva, E., Mayser, J. P., Marzocchi, A., Modestou, S., Ochoa, D., Simon, D., Tulbure, M., Van Den Berg, B., Van Der Schee, M., De Lange, G., Ellam, R., Govers, R., Gutjahr, M., Hilgen, F., Kouwenhoven, T., Lofi, J., Meijer, P., Sierro, F.J., Bachiri, N., Barhoun, N., Alami, A. C., Chacon, B., Flores, J.A., Gregory, J., Howard, J., Lunt, D., Ochoa, M., Pancost, R., Vincent, S., Yousfi, M.Z., 2015. Evolution of the Late Miocene Mediterranean–Atlantic gateways and their impact on regional and global environmental change. Earth Sci. Rev. 150, 365–392.
Fortuin, A.R., Krijgsman, W., 2003. The Messinian of the Nijar Basin (SE Spain): Sedimentation, depositional environments and paleogeographic evolution. Sediment. Geol. 160 (1–3), 213–242.
Frigola, J., Moreno, A., Cacho, I., Canals, M., Sierro, F., Flores, J., Grimalt, J., 2008. Evidence of abrupt changes in Western Mediterranean Deep Water circulation during the last 50 kyr: a high-resolution marine record from the Balearic Sea. Quat. Int. 181 (1), 88–104.
Garcia-Castellanos, D., Villaseñor, A., 2011. Messinian salinity crisis regulated by competing tectonics and erosion at the Gibraltar arc. Nature 480 (7377), 359.
Gebhardt, H., 1999. Middle to Upper Miocene benthonic foraminiferal palaeoecology of the tap Marls (Alicante Province, SE Spain) and its palaeoceanographic implications. Palaeogeogr. Palaeoclimatol. Palaeoecol. 145 (1–3), 141–156.
Gibson, T.G., 1989. Planktonic benthonic foraminiferal ratios: modern patterns and Tertiary applicability. Mar. Micropaleontol. 15 (1–2), 29–52.
Glacon, G., Grazzini, C.V., Iaccarino, S., Rehault, J.-P., Randrianasolo, A., Sierro, J.F., Weaver, P., Channell, J., Torii, M., Hawthorne, T., 1990. Planktonic foraminiferal events and stable isotope records in the upper Miocene, Site 654. In: Kastens, K.A., Mascle, J., et al. (Eds.), Proc. ODP, Sci. Results, 107: College Station, TX (Ocean Drilling Program), pp. 415–427. https://doi.org/10.2973/odp.proc.sr.107.157.1990.
Gooday, A.J., 2003. Benthic foraminifera (Protista) as tools in deep-water palaeoceanography: environmental influences on faunal characteristics. Adv. Mar. Biol. 46, 1–90.
Guerra-Merchán, A., Serrano, F., Garcés, M., Gofas, S., Esu, D., Gliozzi, E., Grossi, F., 2010. Messinian Lago-Mare deposits near the strait of Gibraltar (Malaga basin, S Spain). Palaeogeogr. Palaeoclimatol. Palaeoecol. 285 (3–4), 264–276.
Hammer, Ø., Harper, D.A., Ryan, P.D., 2001. PAST: Paleontological statistics software package for education and data analysis. Palaeontol. Electron. 4 (1), 9.
Harff, J., Endler, R., Emelyanov, E., Kotov, S., Leipe, T., Moros, M., Olea, R., Tomczak, M., Witkowski, A., 2011. Late Quaternary Climate Variations Reflected in Baltic Sea Sediments., the Baltic Sea Basin. Springer, Berlin, Heidelberg, pp. 99–132.
Hennekam, R., Jilbert, T., Schnetger, B., de Lange, G.J., 2014. Solar forcing of Nile discharge and sapropel S1 formation in the early to middle Holocene eastern Mediterranean. Paleoceanography 29 (5), 343–356.
Herbert, T.D., Lawrence, K.T., Tzanova, A., Peterson, L.C., Caballero-Gill, R., Kelly, C.S., 2016. Late Miocene global cooling and the rise of modern ecosystems. Nat. Geosci. 9 (11), 843–847.
Herguera, J.C., 1992. Deep-sea benthic foraminifera and biogenic opal: glacial to postglacial productivity changes in the western equatorial Pacific. Mar. Micropaleontol. 19 (1–2), 79–98.
Herguera, J., 2000. Last glacial paleoproductivity patterns in the eastern equatorial Pacific: benthic foraminifera records. Mar. Micropaleontol. 40 (3), 259–275.
Hilgen, F., Krijgsman, W., Langereis, C., Lourens, L., Santarelli, A., Zachariasse, W., 1995. Extending the astronomical (polarity) time scale into the Miocene. Earth Planet. Sci. Lett. 136, 495–510.
Hilgen, F., Bissoli, L., Iaccarino, S., Krijgsman, W., Meijer, R., Negri, A., Villa, G., 2000. Integrated stratigraphy and astrochronology of the Messinian GSSP at Oued Akrech (Atlantic Morocco). Earth Planet. Sci. Lett. 182 (3–4), 237–251.
Hillaire-Marcel, C., Ravelo, A., 2007. The use of oxygen and carbon isotopes of foraminifera in paleoceanography. Burlington: Elsevier Science. In: Hillaire-Marcel, C., De Vernal, A. (Eds.), Developments in Marine Geology: Proxies in Late Cenozoic Paleoceanography.
Hoang, V.L., Clift, P.D., Schwab, A.M., Huuse, M., Nguyen, D.A., Zhen, S., 2010. Large-scale erosional response of SE Asia to monsoon evolution reconstructed from sedimentary records of the Song Hong-Yinggehai and Qiongdongnan basins, South China Sea. Geol. Soc. Lond., Spec. Publ. 342 (1), 219–244.
Hodell, D.A., Venz-Curtis, K.A., 2006. Late Neogene history of Deepwater ventilation in the Southern Ocean. Geochem. Geophys. Geosyst. 7 (9).
Hodell, D.A., Benson, R.H., Kent, D.V., Boersma, A., Rakic-El Bied, K., 1994. Magnetostratigraphic, biostratigraphic, and stable isotope stratigraphy of an Upper Miocene drill core from the Salé Briqueterie (northwestern Morocco): a high-resolution chronology for the Messinian stage. Paleoceanography 9 (6), 835–855.
Hodell, D.A., Curtis, J.H., Sierro, F.J., Raymo, M.E., 2001. Correlation of late Miocene to early Pliocene sequences between the Mediterranean and North Atlantic. Paleoceanography 16 (2), 164–178.
Holbourn, A., Kuhnt, W., Schulz, M., Flores, J.-A., Andersen, N., 2007. Orbitally-paced climate evolution during the middle Miocene "Monterey" carbon-isotope excursion. Earth Planet. Sci. Lett. 261 (3–4), 534–550.
Holbourn, A.E., Kuhnt, W., Clemens, S.C., Kochhann, K.G., Jöhnck, J., Lübbers, J., Andersen, N., 2018. Late Miocene climate cooling and intensification of southeast Asian winter monsoon. Nat. Commun. 9 (1), 1–13.
Holbourn, A., Kuhnt, W., Clemens, S.C., Heslop, D., 2021. A~ 12 Myr Miocene Record of East Asian Monsoon variability from the South China Sea. Paleoceanogr. Paleoclimatol. 36 (7) e2021PA004267.
Hsü, K.J., Ryan, W.B.F., Cita, M.B., 1973. Late miocene desiccation of the mediterranean. Nature 242 (5395), 240–244.
Hüsing, S., Kuiper, K., Link, W., Hilgen, F.J., Krijgsman, W., 2009. The upper Tortonian–lower Messinian at Monte dei Corvi (Northern Apennines, Italy): completing a Mediterranean reference section for the Tortonian stage. Earth Planet. Sci. Lett. 282 (1–4), 140–157.
Iaccarino, S.M., Bertini, A., Di Stefano, A., Ferraro, L., Gennari, R., Grossi, F., Lirer, F., Manzi, V., Menichetti, E., Ricci Lucchi, M., Taviani, M., 2008. The Trave section (Monte dei Corvi, Ancona, Central Italy): an integrated paleontological study of the Messinian deposits. Stratigraphy 5 (3–4), 281–306.
Jimenez-Espejo, F.J., Martinez-Ruiz, F., Sakamoto, T., Iijima, K., Gallego-Torres, D., Harada, N., 2007. Paleoenvironmental changes in the western Mediterranean since the last glacial maximum: high resolution multiproxy record from the Algero–Balearic basin. Palaeogeogr. Palaeoclimatol. Palaeoecol. 246 (2–4), 292–306.
Jorissen, F.J., 1987. The distribution of benthic foraminifera in the Adriatic Sea. Mar. Micropaleontol. 12, 21–48.
Jorissen, F.J., de Stigter, H.C., Widmark, J.G., 1995. A conceptual model explaining benthic foraminiferal microhabitats. Mar. Micropaleontol. 26 (1–4), 3–15.
Jorissen, F., Fontanier, C., Thomas, E., 2007. Paleoceanographical Proxies Based on Deep-Sea Benthic Foraminiferal Assemblage Characteristics, 1 (07) doi: 10.1016. S1572-5480 (07): 01012-3.
Kaiho, K., Lamolda, M.A., 1999. Catastrophic extinction of planktonic foraminifera at the Cretaceous-Tertiary boundary evidenced by stable isotopes and foraminiferal abundance at Caravaca, Spain. Geology 27 (4), 355–358.
Kaminski, M.A., Kender, S., Ciurej, A., Balc, R., Setoyama, E., 2013. Pliocene agglutinated benthic foraminifera from Site U1341 in the Bering Sea (IODP Expedition 323). Geol. Quart. 57 (2), 335–342.
Karami, M., De Leeuw, A., Krijgsman, W., Meijer, P.T., Wortel, M., 2011. The role of gateways in the evolution of temperature and salinity of semi-enclosed basins: an oceanic box model for the Miocene Mediterranean Sea and Paratethys. Glob. Planet. Chang. 79 (1–2), 73–88.
Kastens, K., Mascle, J., Auroux, C., Bonatti, E., Broglia, C., Channell, J., Curzi, P., Emeis, K.-C., Glaçon, G., Hasegawa, S., 1988. ODP Leg 107 in the Tyrrhenian Sea: insights into passive margin and back-arc basin evolution. Geol. Soc. Am. Bull. 100 (7), 1140–1156.
Katz, M.E., Thunell, R.C., 1984. Benthic foraminiferal biofacies associated with Middle Miocene to early Pliocene oxygen-deficient conditions in the eastern Mediterranean. J. Foraminiferal Res. 14 (3), 187–202.
Koho, K., García, R.D., De Stigter, H., Epping, E., Koning, E., Kouwenhoven, T., Van der Zwaan, G., 2008. Sedimentary labile organic carbon and pore water redox control on species distribution of benthic foraminifera: A case study from Lisbon–Setúbal Canyon (southern Portugal). Prog. Oceanogr. 79 (1), 55–82.
Konijnendijk, T., Ziegler, M., Lourens, L., 2014. Chronological constraints on Pleistocene sapropel depositions from high-resolution geochemical records of ODP Sites 967 and 968. Newsl. Stratigr. 47 (3), 263–282.
Kontakiotis, G., Besiou, E., Antonarakou, A., Zarkogiannis, S., Kostis, A., Mortyn, P., Moissette, P., Cornée, J.-J., Schulbert, C., Drinia, H., 2019. Decoding Sea surface and

paleoclimate conditions in the eastern Mediterranean over the Tortonian-Messinian transition. Palaeogeogr. Palaeoclimatol. Palaeoecol. 534, 109312.
Kouwenhoven, T., Seidenkrantz, M.-S., Van der Zwaan, G., 1999. Deep-water changes: the near-synchronous disappearance of a group of benthic foraminifera from the late Miocene Mediterranean. Palaeogeogr. Palaeoclimatol. Palaeoecol. 152 (3–4), 259–281.
Kouwenhoven, T.J., Hilgen, F.J., Van Der Zwaan, G.J., 2003. Late Tortonian–early Messinian stepwise disruption of the Mediterranean–Atlantic connections: constraints from benthic foraminiferal and geochemical data. Palaeogeogr. Palaeoclimatol. Palaeoecol. 198 (3–4), 303–319.
Kouwenhoven, T., Morigi, C., Negri, A., Giunta, S., Krijgsman, W., Rouchy, J.-M., 2006. Paleoenvironmental evolution of the eastern Mediterranean during the Messinian: Constraints from integrated microfossil data of the Pissouri Basin (Cyprus). Mar. Micropaleontol. 60 (1), 17–44.
Krijgsman, W., Hilgen, F., Langereis, C., Zachariasse, W., 1994. The age of the Tortonian/Messinian boundary. Earth Planet. Sci. Lett. 121, 533–547.
Krijgsman, W., Hilgen, F., Negri, A., Wijbrans, J., Zachariasse, W., 1997. The Monte del Casino section (northern Apennines, Italy): a potential Tortonian/Messinian boundary stratotype? Palaeogeogr. Palaeoclimatol. Palaeoecol. 133 (1–2), 27–47.
Krijgsman, W., Langereis, C., Zachariasse, W., Boccaletti, M., Moratti, G., Gelati, R., Iaccarino, S., Papani, G., Villa, G., 1999. Late Neogene evolution of the Taza–Guercif Basin (Rifian Corridor, Morocco) and implications for the Messinian salinity crisis. Mar. Geol. 153 (1–4), 147–160.
Krijgsman, W., Blanc-Valleron, M.-M., Flecker, R., Hilgen, F., Kouwenhoven, T., Merle, D., Orszag-Sperber, F., Rouchy, J.-M., 2002. The onset of the Messinian salinity crisis in the Eastern Mediterranean (Pissouri Basin, Cyprus). Earth Planet. Sci. Lett. 194 (3–4), 299–310.
Krijgsman, W., Leewis, M.E., Garcés, M., Kouwenhoven, T.J., Kuiper, K.F., Sierro, F.J., 2006. Tectonic control for evaporite formation in the Eastern Betics (Tortonian; Spain). Sediment. Geol. 188, 155–170.
Krijgsman, W., Capella, W., Simon, D., Hilgen, F.J., Kouwenhoven, T.J., Meijer, P.T., Sierro, F.J., Tulbure, M.A., van den Berg, B.C., van der Schee, M., 2018. The Gibraltar corridor: watergate of the messinian salinity crisis. Mar. Geol. 403, 238–246.
Kucera, M., 2007. Planktonic foraminifera as tracers of past oceanic environments. In: Developments in Marine Geology, Chapter 6, pp. 213–262.
Langer, M.R., 1993. Epiphytic foraminifera. Mar. Micropaleontol. 20 (3–4), 235–265.
Larrasoaña, J., Roberts, A., Rohling, E., Winklhofer, M., Wehausen, R., 2003. Three million years of monsoon variability over the northern Sahara. Clim. Dyn. 21 (7–8), 689–698.
Lascaratos, A., Roether, W., Nittis, K., Klein, B., 1999. Recent changes in deep water formation and spreading in the eastern Mediterranean Sea: a review. Prog. Oceanogr. 44 (1–3), 5–36.
Laskar, J., Robutel, P., Joutel, F., Gastineau, M., Correia, A., Levrard, B., 2004. A long-term numerical solution for the insolation quantities of the Earth. Astron. Astrophys. 428 (1), 261–285.
Laube-Lenfant, E., Pierre, C., 1994. Variability of delta-c-13 of sigma-co2 in ocean waters of the equatorial pacific. Oceanol. Acta 17 (6), 633–641.
Lirer, F., Foresi, M., Iaccarino, S., Salvatorini, G., Turco, E., Cosentino, C., Sierro, F.J., Caruso, A., 2019. Mediterranean Neogene planktonic foraminifer biozonation and biochronology. Earth Sci. Rev. 196, 102869.
Lisiecki, L.E., Raymo, M.E., 2005. A Pliocene-Pleistocene stack of 57 globally distributed benthic δ18O records. Paleoceanography 20 (1), 1–17.
Loubère, P., 1996. The surface ocean productivity and bottom water oxygen signals in deep water benthic foraminiferal assemblages. Mar. Micropaleontol. 28 (3–4), 247–261.
Lourens, L.J., Antonarakou, A., Hilgen, F., Van Hoof, A., Vergnaud-Grazzini, C., Zachariasse, W., 1996. Evaluation of the Plio-Pleistocene astronomical timescale. Paleoceanography 11 (4), 391–413.
Lückge, A., Horsfield, B., Littke, R., Scheeder, G., 2002. Organic matter preservation and sulfur uptake in sediments from the continental margin off Pakistan. Org. Geochem. 33 (4), 477–488.
Lutze, G., Coulbourn, W., 1984. Recent benthic foraminifera from the continental margin of Northwest Africa: community structure and distribution. Mar. Micropaleontol. 8 (5), 361–401.
Lutze, G., Thiel, H., 1989. Epibenthic foraminifera from elevated microhabitats; Cibicidoides wuellerstorfi and Planulina ariminensis. J. Foraminiferal Res. 19 (2), 153–158.
Mackensen, A., Sejrup, H., Jansen, E., 1985. The distribution of living benthic foraminifera on the continental slope and rise off Southwest Norway. Mar. Micropaleontol. 9 (4), 275–306.
Mackensen, A., Fu, D., Grobe, H., Schmiedl, G., 1993. Benthic foraminiferal assemblages from the eastern South Atlantic Polar Front region between 35 and 57 S: distribution, ecology and fossilization potential. Mar. Micropaleontol. 22 (1–2), 33–69.
Manzi, V., Iaccarino, S.M., Lugli, S., Roveri, M., 2008. Messinian salinity crisis revisited-II: New views of a vanished ocean. Stratigraphy 5 (3–4), 225–226.
Manzi, V., Gennari, R., Hilgen, F., Krijgsman, W., Lugli, S., Roveri, M., Sierro, F.J., 2013. Age refinement of the Messinian salinity crisis onset in the Mediterranean. Terra Nova 25 (4), 315–322.
Martín, J.M., Braga, J.C., Betzler, C., 2001. The Messinian Guadalhorce corridor: the last northern, Atlantic–Mediterranean gateway. Terra Nova 13 (6), 418–424.
Martín, J.M., Puga-Bernabéu, A., Aguirre, J., Braga, J.C., 2014. Miocene Atlantic-Mediterranean seaways in the Betic Cordillera (Southern Spain). Rev. Soc. Geol. Esp. 27 (1), 175–186.
Martinez-Ruiz, F., Kastner, M., Gallego-Torres, D., Rodrigo-Gámiz, M., Nieto-Moreno, V., Ortega-Huertas, M., 2015. Paleoclimate and paleoceanography over the past 20,000 yr in the Mediterranean Sea Basins as indicated by sediment elemental proxies. Quat. Sci. Rev. 107, 25–46.
Marzocchi, A., Lunt, D., Flecker, R., Bradshaw, C., Farnsworth, A., Hilgen, F., 2015. Orbital control on late Miocene climate and the North African monsoon: insight from an ensemble of sub-precessional simulations. Clim. Past 11 (10), 1271–1295.
Masqué, P., Fabres, J., Canals, M., Sanchez-Cabeza, J., Sanchez-Vidal, A., Cacho, I., Calafat, A., Bruach, J., 2003. Accumulation rates of major constituents of hemipelagic sediments in the deep Alboran Sea: a centennial perspective of sedimentary dynamics. Mar. Geol. 193 (3–4), 207–233.
MEDARGroup, 2002. Medatlas 2002: Mediterranean and Black Sea Database of Temper-Ature, Salinity and Biochemical Parameters—Climatological Atlas. IFREMER, Brest, France.
Meijer, P.T., 2006. A box model of the blocked-outflow scenario for the Messinian Salinity Crisis. Earth Planet. Sci. Lett. 248 (1–2), 486–494.
Murat, A., 1999. Pliocene-Pleistocene occurrence of sapropels in the Western Mediterranean Sea and their relation to Eastern Mediterranean Sapropels. In: Proceedings of the Ocean Drilling Program, Scientific Results, 41, pp. 519–527.
Murray, J., 1991. Ecology and Palaeoecology of Benthic Foraminifera: Longman Scientific and Technical. Harlow, Essex, UK.
Murray, J.W., 2006. Ecology and Applications of Benthic Foraminifera. Cambridge University Press.
Myers, P.G., Haines, K., Rohling, E.J., 1998. Modeling the paleocirculation of the Mediterranean: the last Glacial Maximum and the Holocene with emphasis on the formation of sapropel S 1. Paleoceanography 13 (6), 586–606.
Naidu, P.D., Malmgren, B.A., 1995. Do benthic foraminifer records represent a productivity index in oxygen minimum zone areas? An evaluation from the Oman Margin, Arabian Sea. Mar. Micropaleontol. 26 (1–4), 49–55.
Nguyen, T.M.P., Petrizzo, M.R., Stassen, P., Speijer, R.P., 2011. Dissolution susceptibility of Paleocene–Eocene planktic foraminifera: Implications for palaeoceanographic reconstructions. Mar. Micropaleontol. 81 (1–2), 1–21.
Ochoa, D., Sierro, F.J., Lofi, J., Maillard, A., Flores, J.-A., Suárez, M., 2015. Synchronous onset of the Messinian evaporite precipitation: first Mediterranean offshore evidence. Earth Planet. Sci. Lett. 427, 112–124.
Osborne, A.H., Marino, G., Vance, D., Rohling, E., 2010. Eastern Mediterranean surface water Nd during Eemian sapropel S5: monitoring northerly (mid-latitude) versus southerly (sub-tropical) freshwater contributions. Quat. Sci. Rev. 29 (19–20), 2473–2483.
Pelum, C., Frerichs, W. and Sliter, W., 1976. Gulf of Mexico deep-water foraminifers in: Wiliam V. Slitter (Ed.). Cushman Found. Form. Res. Spec., 14: 1–124.
Pérez-Asensio, J.N., Aguirre, J., Schmiedl, G., Civis, J., 2012a. Messinian paleoenvironmental evolution in the lower Guadalquivir Basin (SW Spain) based on benthic foraminifera. Palaeogeogr. Palaeoclimatol. Palaeoecol. 326, 135–151.
Pérez-Asensio, J.N., Aguirre, J., Schmiedl, G., Civis, J., 2012b. Impact of restriction of the Atlantic-Mediterranean gateway on the Mediterranean Outflow Water and eastern Atlantic circulation during the Messinian. Paleoceanography 27 (3).
Pérez-Asensio, J.N., Frigola, J., Pena, L.D., Sierro, F.J., Reguera, M.I., Rodríguez-Tovar, F.J., Dorador, J., Asioli, A., Kuhlmann, J., Huhn, K., 2020. Changes in western Mediterranean thermohaline circulation in association with a deglacial Organic Rich Layer formation in the Alboran Sea. Quat. Sci. Rev. 228, 106075.
Pérez-Folgado, M., Sierro, F.J., Bárcena, M.A., Flores, J.A., Vázquez, A., Utrilla, R., Hilgen, F.J., Krijgsman, W., Filippelli, G.M., 2003. Western versus eastern Mediterranean paleoceanographic response to astronomical forcing: a high-resolution microplankton study of precession-controlled sedimentary cycles during the Messinian. Palaeogeogr. Palaeoclimatol. Palaeoecol. 190, 317–334.
Pérez-Folgado, M., Sierro, F.J., Flores, J.A., Grimalt, J.O., Zahn, R., 2004. Paleoclimatic variations in foraminifer assemblages from the Alboran Sea (Western Mediterranean) during the last 150 ka in ODP Site 977. Mar. Geol. 212 (1–4), 113–131.
Pflum, C.E., Frerichs, W.E., Sliter, W.V., 1976. Gulf of Mexico Deep-Water Foraminifers. Cushman Foundation for Foraminiferal Research, p. 14.
Pierre, C., 1999. The oxygen and carbon isotope distribution in the Mediterranean water masses. Mar. Geol. 153 (1–4), 41–55.
Pinardi, N., Masetti, E., 2000. Variability of the large scale general circulation of the Mediterranean Sea from observations and modelling: a review. Palaeogeogr. Palaeoclimatol. Palaeoecol. 158 (3–4), 153–173.
Pinardi, N., Cessi, P., Borile, F., Wolfe, C.L., 2019. The Mediterranean Sea overturning circulation. J. Phys. Oceanogr. 49 (7), 1699–1721.
Poli, M.S., Meyers, P.A., Thunell, R.C., Capodivacca, M., 2012. Glacial-interglacial variations in sediment organic carbon accumulation and benthic foraminiferal assemblages on the Bermuda rise (ODP Site 1063) during MIS 13 to 10. Paleoceanography 27 (3).
Pound, M.J., Haywood, A.M., Salzmann, U., Riding, J.B., 2012. Global vegetation dynamics and latitudinal temperature gradients during the Mid to Late Miocene (15.97–5.33 Ma). Earth Sci. Rev. 112 (1–2), 1–22.
Powley, H.R., Cappellen, P., Krom, M.D., 2017. Nutrient cycling in the Mediterranean Sea: the key to understanding how the unique marine ecosystem functions and responds to anthropogenic pressures. Mediterranean Identities—Environment, Society. Culture. InTech, 47–77.
Riveiros, N.V., Waelbroeck, C., Skinner, L., Roche, D.M., Duplessy, J.-C., Michel, E., 2010. Response of South Atlantic deep waters to deglacial warming during Terminations V and I. Earth Planet. Sci. Lett. 298 (3–4), 323–333.
Rodrigo-Gámiz, M., Martínez-Ruiz, F., Rodríguez-Tovar, F.J., Jiménez-Espejo, F.J., Pardo-Igúzquiza, E., 2014. Millennial-to centennial-scale climate periodicities and forcing mechanisms in the westernmost Mediterranean for the past 20,000 yr. Quat. Res. 81 (1), 78–93.

Roger, S., Münch, P., Cornée, J., Saint Martin, J., Féraud, G., Pestrea, S., Conesa, G., Moussa, A.B., 2000. 40Ar/39Ar dating of the pre-evaporitic Messinian marine sequences of the Melilla basin (Morocco): a proposal for some biosedimentary events as isochrons around the Alboran Sea. Earth Planet. Sci. Lett. 179 (1), 101–113.
Rogerson, M., Cacho, I., Jimenez-Espejo, F., Reguera, M., Sierro, F.J., Martinez-Ruiz, F., Frigola, J., Canals, M., 2008. A dynamic explanation for the origin of the western Mediterranean organic-rich layers. Geochem. Geophys. Geosyst. 9 (7).
Rogerson, M., Bigg, G.R., Rohling, E., Ramirez, J., 2012. Vertical density gradient in the eastern North Atlantic during the last 30,000 years. Clim. Dyn. 39 (3–4), 589–598.
Rohling, E.J., Cooke, S., 1999. Stable oxygen and carbon isotopes in foraminiferal carbonate shells. In: Modern Foraminifera. Springer, pp. 239–258.
Rohling, E.J., De Rijk, S., 1999. Holocene climate Optimum and last Glacial Maximum in the Mediterranean: the marine oxygen isotope record. Mar. Geol. 153 (1–4), 57–75.
Rohling, E.J., Abu-Zied, R., Casford, J., Hayes, A., Hoogakker, B., 2009. The marine environment: present and past. Phys. Geogr. Mediterranean 33–67.
Rohling, E., Marino, G., Grant, K., 2015. Mediterranean climate and oceanography, and the periodic development of anoxic events (sapropels). Earth Sci. Rev. 143, 62–97.
Rossignol-Strick, M., 1985. Mediterranean Quaternary sapropels, an immediate response of the African monsoon to variation of insolation. Palaeogeogr. Palaeoclimatol. Palaeoecol. 49 (3–4), 237–263.
Rothwell, R.G., 2015. Twenty years of XRF core scanning marine sediments: what do geochemical proxies tell us?. In: Micro-XRF Studies of Sediment Cores. Springer, pp. 25–102.
Roveri, M., Flecker, R., Krijgsman, W., Lofi, J., Lugli, S., Manzi, V., Sierro, F.J., Bertini, A., Camerlenghi, A., De Lange, G., 2014a. The Messinian Salinity Crisis: past and future of a great challenge for marine sciences. Mar. Geol. 352, 25–58.
Roveri, M., Lugli, S., Manzi, V., Gennari, R., Schreiber, B.C., 2014b. High-resolution strontium isotope stratigraphy of the messinian deep mediterranean basins: Implications for marginal to central basins correlation. Mar. Geol. 349, 113–125.
Ryan, W.B., 1976. Quantitative evaluation of the depth of the western Mediterranean before, during and after the Late Miocene salinity crisis. Sedimentology 23 (6), 791–813.
Santarelli, A., Brinkhuis, H., Hilgen, F., Lourens, L., Versteegh, G., Visscher, H., 1998. Orbital signatures in a Late Miocene dinoflagellate record from Crete (Greece). Mar. Micropaleontol. 33 (3–4), 273–297.
Schlitzer, R., 2015. Data analysis and visualization with Ocean Data View. CMOS Bull. SCMO 43 (1), 9–13.
Schlitzer, R., Roether, W., Oster, H., Junghans, H.-G., Hausmann, M., Johannsen, H., Michelato, A., 1991. Chlorofluoromethane and oxygen in the Eastern Mediterranean. Deep Sea Res. Part A. Ocean. Res. Papers 38 (12), 1531–1551.
Schönfeld, J., 1997. The impact of the Mediterranean Outflow Water (MOW) on benthic foraminiferal assemblages and surface sediments at the southern Portuguese continental margin. Mar. Micropaleontol. 29 (3–4), 211–236.
Schuster, M., 2006. The Age of the Sahara Desert. Science 311 (5762), 821.
Seidenkrantz, M.-S., Kouwenhoven, T., Jorissen, F., Shackleton, N., Van der Zwaan, G., 2000. Benthic foraminifera as indicators of changing Mediterranean–Atlantic water exchange in the late Miocene. Mar. Geol. 163 (1–4), 387–407.
Sen Gupta, B.K., Machain-Castillo, M.L., 1993a. Benthic foraminifera in oxygen-poor habitats, 20 (3–4), 183–201.
Sen Gupta, B.K., Machain-Castillo, M.L., 1993b. Benthic foraminifera in oxygen-poor habitats. Mar. Micropaleontol. 20 (3–4), 183–201.
Sepulchre, P., Ramstein, G., Fluteau, F., Schuster, M., Tiercelin, J.-J., Brunet, M., 2006. Tectonic uplift and Eastern Africa aridification. Science 313 (5792), 1419–1423.
Sgarrella, F., Moncharmont Zei, M., 1993. Benthic foraminifera of the Gulf of Naples (Italy): Systematics and autoecology. In: Bollettino della Società Paleontologica Italiana(2).
Shannon, C.E., 1948. A mathematical theory of communication. Bell Syst. Tech. J. 27 (3), 379–423.
Sierro, F.J., Hilgen, F.J., Krijgsman, W., Flores, J.A., 2001. The Abad composite (SE Spain): a messinian reference section for the mediterranean and the APTS, 168 (1–2), 141–169.
Sierro, F.J., Flores, J.A., Francés, G., Vazquez, A., Utrilla, R., Zamarreño, I., Erlenkeuser, H., Barcena, M.A., 2003. Orbitally-controlled oscillations in planktic communities and cyclic changes in western Mediterranean hydrography during the Messinian. Palaeogeogr. Palaeoclimatol. Palaeoecol. 190, 289–316.
Simon, D., Marzocchi, A., Flecker, R., Lunt, D.J., Hilgen, F.J., Meijer, P.T., 2017. Quantifying the Mediterranean freshwater budget throughout the late Miocene: New implications for sapropel formation and the Messinian Salinity Crisis. Earth Planet. Sci. Lett. 472, 25–37.
Simon, D., Meijer, P., 2015. Dimensions of the Atlantic–Mediterranean connection that caused the Messinian Salinity Crisis. Mar. Geol. 364, 53–64.
Spellerberg, I.F., Fedor, P.J., 2003. A tribute to Claude Shannon (1916–2001) and a plea for more rigorous use of species richness, species diversity and the 'Shannon–Wiener'Index. Glob. Ecol. Biogeogr. 12 (3), 177–179.
Spero, H.J., Lea, D.W., 1996. Experimental determination of stable isotope variability in Globigerina bulloides: implications for paleoceanographic reconstructions. Mar. Micropaleontol. 28 (3–4), 231–246.
Sprovieri, R., Di Stefano, E., Caruso, A., Bonomo, S., 1996. High resolution stratigraphy in the Messinian Tripoli Formation in Sicily. Paleopelagos 6, 415–435.
Sprovieri, M., Bellanca, A., Neri, R., Mazzola, S., Bonanno, A., Patti, B., Sorgente, R., 1999. Astronomical calibration of late Miocene stratigraphic events and analysis of precessionally driven paleoceanographic changes in the Mediterranean basin. Mem. Soc. Geol. Ital. 54, 7–24.
Stommel, H., Bryden, H., Mangelsdorf, P., 1973. Does some of the Mediterranean outflow come from great depth? Pure Appl. Geophys. 105 (1), 879–889.
Tanner, T., Hernández-Almeida, I., Drury, A.J., Guitián, J., Stoll, H., 2020. Decreasing atmospheric CO2 during the late Miocene Cooling. Paleoceanogr. Paleoclimatol. 35 e2020PA003925.
Theocharis, A., Georgopoulos, D., 1993. Dense water formation over the Samothraki and Limnos Plateaux in the North Aegean Sea (eastern Mediterranean Sea). Cont. Shelf Res. 13 (8–9), 919–939.
Topper, R., Meijer, P.T., 2015. Changes in Mediterranean circulation and water characteristics due to restriction of the Atlantic connection: a high-resolution ocean model. Clim. Past 11 (2), 233–251.
Tulbure, M., Capella, W., Barhoun, N., Flores, J., Hilgen, F., Krijgsman, W., Kouwenhoven, T., Sierro, F.J., Yousfi, M.Z., 2017. Age refinement and basin evolution of the North Rifian Corridor (Morocco): no evidence for a marine connection during the Messinian Salinity Crisis. Palaeogeogr. Palaeoclimatol. Palaeoecol. 485, 416–432.
Tzanova, A., Herbert, T.D., Peterson, L., 2015. Cooling Mediterranean Sea surface temperatures during the late Miocene provide a climate context for evolutionary transitions in Africa and Eurasia. Earth Planet. Sci. Lett. 419, 71–80.
Van den Berg, B.C.J., Sierro, F.J., Hilgen, F.J., Flecker, R., Larrasoaña, J.C., Krijgsman, W., Flores, J.A., Mata, M.P., Bellido Martín, E., Civis, J., González-Delgado, J.A., 2015. Astronomical tuning for the upper Messinian Spanish Atlantic margin: Disentangling basin evolution, climate cyclicity and MOW, 135, 89–103.
Van den Berg, B.C.J., Sierro, F.J., Hilgen, F.J., Flecker, R., Larrasoaña, J.C., Krijgsman, W., Flores, J.A., Mata, M.P., 2018. Imprint of Messinian Salinity Crisis events on the Spanish Atlantic margin. Newsl. Stratigr. 51 (1), 93–115.
Van der Laan, E., Snel, E., De Kaenel, E., Hilgen, F., Krijgsman, W., 2006. No major deglaciation across the Miocene-Pliocene boundary: integrated stratigraphy and astronomical tuning of the Loulja sections (Bou Regreg area, NW Morocco). Paleoceanography 21 (3).
Van Der Laan, E., Hilgen, F.J., Lourens, L.J., De Kaenel, E., Gaboardi, S., Iaccarino, S., 2012. Astronomical forcing of Northwest African climate and glacial history during the late Messinian (6.5–5.5Ma). Palaeogeogr. Palaeoclimatol. Palaeoecol. 313-314, 107–126.
Van der Schee, M., Van den Berg, B.C., Capella, W., Simon, D., Sierro, F.J., Krijgsman, W., 2018. New age constraints on the western Betic intramontane basins: a late Tortonian closure of the Guadalhorce Corridor? Terra Nova 30 (5), 325–332.
Van der Zwaan, G., Jorissen, F., De Stigter, H., 1990. The depth dependency of planktonic/benthic foraminiferal ratios: constraints and applications. Mar. Geol. 95 (1), 1–16.
Van der Zwaan, G., Duijnstee, I., Den Dulk, M., Ernst, S., Jannink, N., Kouwenhoven, T., 1999. Benthic foraminifers: proxies or problems?: a review of paleocological concepts. Earth Sci. Rev. 46 (1–4), 213–236.
Van Hinsbergen, D.J.J., Kouwenhoven, T.J., Van Der Zwaan, G.J., 2005. Paleobathymetry in the backstripping procedure: Correction for oxygenation effects on depth estimates, 221 (3–4), 245–265.
Van Marle, L., 1988. Bathymetric distribution of benthic foraminifera on the Australian-Irian Jaya continental margin, eastern Indonesia. Mar. Micropaleontol. 13 (2), 97–152.
Vázquez, A., Utrilla, R., Zamarreno, I., Sierro, F., Flores, J., Francés, G., Barcena, M., 2000. Precession-related sapropelites of the Messinian Sorbas Basin (South Spain): paleoenvironmental significance. Palaeogeogr. Palaeoclimatol. Palaeoecol. 158 (3–4), 353–370.
Violanti, D., Dela Pierre, F., Trenkwalder, S., Lozar, F., Clari, P., Irace, A., D'Atri, A., 2011. Biostratigraphic and palaeoenvironmental analyses of the Messinian/Zanclean boundary and Zanclean succession in the Moncucco quarry (Piedmont, northwestern Italy). Bull. Soc. géol. France 182 (2), 149–162.
Wefer, G., Berger, W.H., 1991. Isotope paleontology: growth and composition of extant calcareous species. Mar. Geol. 100 (1–4), 207–248.
Weinkauf, M.F., Milker, Y., 2018. The effect of size fraction in analyses of benthic foraminiferal assemblages: a case study comparing assemblages from the> 125 and> 150 μm size fractions. Front. Earth Sci. 6, 37.
Weltje, G.J., Tjallingii, R., 2008. Calibration of XRF core scanners for quantitative geochemical logging of sediment cores: Theory and application. Earth Planet. Sci. Lett. 274 (3–4), 423–438.
Wright, R., 1978. 41. Neogene paleobathymetry of the Mediterranean based on benthic foraminifers from DSDP Leg 42a. Initial Rep. DSDP 42, 837–847.
Zavatarielli, M., Mellor, G.L., 1995. A numerical study of the Mediterranean Sea circulation. J. Phys. Oceanogr. 25 (6), 1384–1414.
Zhang, Y.G., Pagani, M., Liu, Z., Bohaty, S.M., DeConto, R., 2013. A 40-million-year history of atmospheric CO2. Philos. Trans. R. Soc. A Math. Phys. Eng. Sci. 371 (2001), 20130096.
Zhang, Z., Ramstein, G., Schuster, M., Li, C., Contoux, C., Yan, Q., 2014. Aridification of the Sahara desert caused by Tethys Sea shrinkage during the late Miocene. Nature 513 (7518), 401–404.